ELECTROCALORIC PROPERTIES OF THE ZR-SUBSTITUTED $BaTiO_3$ – $Na_{0.5}Bi_{0.5}TiO_3$ CERAMICS

A Thesis Submitted to
The Graduate School of Engineering and Science of
İzmir Institute of Technology
in Partial Fulfillment of the Requirements for the Degree of

MASTER OF SCIENCES

In Materials Science and Engineering

by
Oğuz AKKAŞOĞLU

December 2023
İZMİR

We approve the thesis of **Oğuz AKKAŞOĞLU**

Examining Committee Members:

Assoc. Prof. Umut ADEM
Department of Materials Science and Engineering, İzmir Institute of Technology

Prof. Dr. Sedat AKKURT
Department of Materials Science and Engineering, İzmir Institute of Technology

Assoc. Prof. Suat Bahar BAŞTÜRK
Department of Metallurgical and Materials Engineering, Manisa Celal Bayar University

8 December 2023

Assoc. Prof. Umut ADEM
Supervisor, Department of
Materials Science and Engineering,
İzmir Institute of Technology

Prof. Dr. Yaşar AKDOĞAN
Head of Department of
Materials Science and Engineering

Prof. Dr. Mehtap EANES
Dean of the Graduate
School of Engineering and Sciences

ACKNOWLEDGEMENT

I would like to express my heartfelt gratitude to my advisor, Asst. Prof. Dr. Umut Adem, for their unwavering support, guidance, and invaluable mentorship throughout the entire research process. Their expertise and dedication played a pivotal role in shaping the direction of this thesis. A special thanks goes to Dr. Merve Günnar Karakaya whose assistance and support were important in the smooth progress of this work. I am sincerely grateful for their patience and willingness to share their knowledge.

I extend my appreciation to my colleagues Efe Batı Güleç, Ece Doğan and Simay Dindar whose insights and collaboration enriched the research experience. Their contributions were invaluable, and I am thankful for the companionship we shared during this academic journey. Their help significantly contributed to the successful completion of this research. I would also like to thank to the Materials Research Center for providing access to their state-of-the-art instruments and facilities. This support was crucial in conducting experiments and gathering essential data for the thesis.

To my friends who provided encouragement, constructive feedback, and a listening ear during challenging times, I extend my deepest thanks. Your friendship has been a source of strength throughout this academic endeavor. Finally, I want to express my profound appreciation to my beloved family. Their unconditional support, understanding, and encouragement, especially in hard times that I faced, sustained me in this academic pursuit. Their vision and dedication brought me to IZTECH. Their love has been my anchor, and I am truly grateful for their presence in my life.

This thesis is a testament to the collective efforts of those mentioned above, and I am sincerely thankful for the positive impact each one of you has had on my academic journey.

ABSTRACT

ELECTROCALORIC PROPERTIES OF THE ZR-SUBSTITUTED $BaTiO_3 - Na_{0.5}Bi_{0.5}TiO_3$ CERAMICS

The aim of this study is to investigate electrocaloric properties and thermodynamic behaviour, obtaining high adiabatic temperature change (ΔT) values with a broad temperature span of zirconium doped barium titanate-sodium bismuth titanate by substitution of Zr into B-site (titanium).

Ceramics are synthesized in a pellet form by solid-state reactions. Chemical composition was $Ba_{0.7}Na_{0.15}Bi_{0.15}Ti_xZr_{1-x}O_3$ (abbreviated as BT-NBT) where x= 0.00, 0.01, 0.02, 0.03, 0.035, 0.04 and 0.05. Phase analysis was conducted by X-ray diffraction method. Microstructural analysis and average grain size determination was performed by Scanning Electron Microscopy. To understand phase transitions and physical behaviours, dielectric measurements are performed. Ferroelectric properties are investigated by using temperature dependent polarization, strain and current-electric field relationships. Electrocaloric measurements are done by using temperature dependent polarization-electric field data. Maxwell relations are used to calculate temperature dependent electrocaloric temperature change, ΔT, and from this data, temperature span, T_{span}, was calculated. It was observed even though Zr substitution into the Ti-site rapidly decreases the Curie temperature and introduces relaxor ferroelectric character to the samples. However, the 1^{st} order like nature of the ferroelectric-paraelectric phase transition at the Curie temperature and, consequently significant ΔT is maintained even for 4 % Zr substituted sample close to room temperature. Temperature span, on the other hand, has a lower value compared to previous works related to barium titanate systems. Electrocaloric efficiency is comparable to other works on Pb-free sytems and these results showed that BT-NBT systems have promising features for electrocaloric cooling technologies.

ÖZET

ZR-KATKILANMIŞ $BaTiO_3$ – $Na_{0.5}Bi_{0.5}TiO_3$ SERAMİKLERİNİN ELEKTROKALORİK ÖZELLİKLERİ

Bu çalışmanın amacı, zirkonyum ile katkılanmış baryum titanat-sodyum bismut titanatın elektrokalorik özelliklerini ve termodinamik davranışını incelemek, perovskite ABO_3 yapısının B-pozisyonuna (titanyum) zirkonyumun katkılanması ile geniş bir sıcaklık aralığında yüksek adyabatik sıcaklık değişimi (ΔT) değerleri elde etmektir.

Seramikler, katı hal tepkimeleri ile pelet formunda sentezlendi. Kimyasal kompozisyon şu şekildedir: $Ba_{0.7}Na_{0.15}Bi_{0.15}Ti_xZr_{1-x}O_3$, burada x= 0.00, 0.01, 0.02, 0.03, 0.035, 0.04 ve 0.05 moldür. Faz analizi X-ışını kırınımı yöntemi ile gerçekleştirilmiştir. Mikroyapısal analiz ve ortalama tane boyu belirleme taramalı elektron mikroskobu ile yapılmıştır. Faz geçişlerini ve fiziksel davranışları anlamak için dielektrik ölçümler yapılmıştır. Ferroelektrik özellikler, sıcaklığa bağlı polarizasyon, gerinim ve akım-elektrik alan ilişkileri kullanılarak incelenmiştir. Elektrokalorik ölçümler, sıcaklığa bağlı polarizasyon-elektrik alan verileri kullanılarak yapılmıştır. Maxwell denklemeler,, sıcaklığa bağlı sıcaklık değişimi, ΔT'yi hesaplamak için kullanılmıştır ve ΔT'nin belli bir değerin üzerinde kaldığı sıcaklık aralığı, T_{span} elde edilmiştir. Zr iyonlarının Titanyum pozisyonuna katkılanması, Curie sıcaklığını çok düşürüp, malzemelerin relaxor gibi davranmasına yol açsa da, ferroelektrik-paraelektrik faz geçişindeki 1. dereceden faz geçişi davranışı ve bunun sonucunda elde edilen kayda değer ΔT değeri, %4 Zr katkılanmış ve faz geçişi oda sıcaklığına yaklaşmış örnekte bile sağlanmış oldu. Diğer yandan görece yüksek elektrokalorik etkinin görüldüğü sıcaklık aralığı, literatürdeki baryum titanat bazlı örneklerde yapılan çalışmalarına kıyasla daha düşük kaldı ama elektrokalorik verimlilik literature kıyasla kayda değer sonuçlar verdi. Tüm bu sonuçlar, BT-NBT sistemlerinin, elektrokalorik soğutma teknolojileri için umut vaat eden özelliklere sahip olduğunu göstermektedir.

TABLE OF CONTENTS

LIST OF FIGURES

Figure **Page**

LIST OF TABLES

CHAPTER 1

INTRODUCTION & MOTIVATION

1.1.Introduction

Cooling technologies have become a vital part of modern life, contributing significantly to our comfort, productivity and preservation of essential goods and services. From air conditioning systems that keep homes and workplaces cool to refrigeration units that store goods. Although they are one of the key parts of daily lives, the widespread adaptation of cooling technologies has raised environmental concerns. These concerns are multidimensional and encompass a range of interconnected issues.

Energy consumption is one of the dimensions of this problem. According to the International Energy Agency's flagship report "Net Zero Roadmap", the energy consumption of space cooling (cooling of workplaces, homes, and public places) out of the overall world's electricity consumption is nearly 10% and by 2050, energy consumption will be doubled to 20%. Figure 1.1 illustrates the energy consumption. By looking at usage, the cooled floor area in buildings in 2022 is 105 billion square meters and by 2050, this value will be nearly 250 billion square meters.("Net Zero Roadmap: A Global Pathway to Keep the 1.5 °C Goal in Reach" 2023) Usage of cooling technologies will be increased so energy consumption will be increased too. The other dimension of the problem is emission of greenhouse gases to atmosphere. Refrigerants, air conditioning units and other uses emit hydrofluorocarbon (HFC) gases that are thousands of times higher than carbon dioxide. HFC gases also have high global warming potentials due to their molecules' short lifetime that fastens the path to the climate change.(Shah et al. 2015)

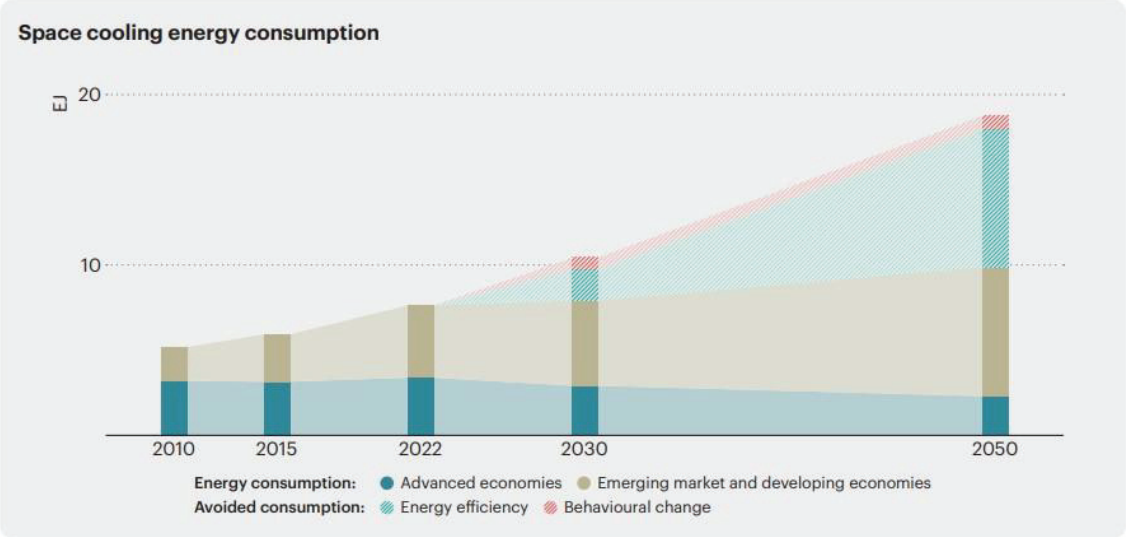

Figure 1.1. Space cooling energy consumption projection

Due to the rising concerns, countries are trying to solve these problems like declaring Kigali Amendment which aims to replace harmful cooling technologies to natural ones that emits other refrigerants such as CO_2 and ammonia.(Heath 2017) However, these kinds of solutions still don't solve problems like energy consumption and entail other side effects such as toxicity and flammability. In these case, new technologies are needed to overcome these problems and concerns for future. New technologies like electrocaloric effect can be a key technology in the future. Electrocaloric materials that possess electrocaloric effect have promising features for cooling technologies to resolve both energy consumption and emission of greenhouse gases. But before understanding electrocaloric materials, ferroelectricity must be explained.

1.2. Ferroelectricity

1.2.1. Definition

A material is said to be ferroelectric if it shows spontaneous polarization and if the direction of the electrical polarization is reversible by applying electric field.(Lines and Glass 2001)

1.2.2. History

In the eighteenth and nineteenth centuries, several scientists such as Gaugain have worked on pyroelectricity, a phenomenon which explains temperature dependent spontaneous electric dipole moment. Step by step, these works led to discovery of piezoelectricity in 1880 by two brothers Paul-Jacques Curie and Pierre Currie who is the husband of Marie Sklodowska-Curie.(Lines and Glass 2001)

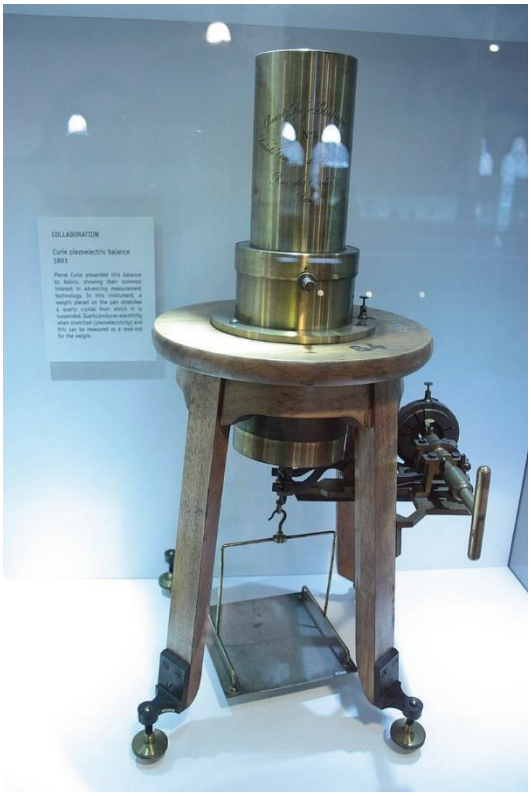

Figure 1.2. Piezoelectric balance represented by Curie.("Piezoelectric Balance Presented by Pierre Curie to Lord Kelvin, Hunterian Museum, Glasgow," n.d.)

The ferroelectrics, on the other hand, were discovered many years later due to lack of any net polarization and unnoticeable pyroelectric and piezoelectric response of the formation domains of differently oriented polarization in single crystals. In 1920, a Czech-origin American scientist named Joseph Valasek discovered the polarization of Rochelle Salt (Sodium potassium tartrate tetrahydrate, $NaKCH_4O_6.4H_2O$). This

polarization could be reversed by an external electric field. He later found that the dielectric properties of Rochelle Salt were very similar in ferromagnetic properties of iron and revealed a hysteresis effect and a Curie Temperature.(Lines and Glass 2001)

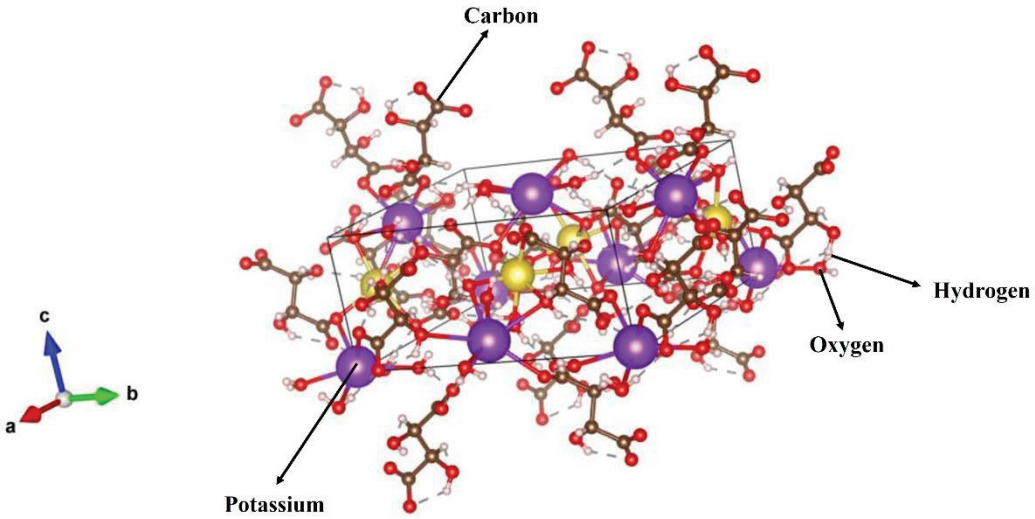

Figure 1.3. Crystal Structure of Rochelle Salt.(Mo et al. 2015)

In these times, ferroelectricity term was not commonly used, and Curie point was referred to the onset of polar ordering up to 1935. Rochelle salt was the only example of ferroelectric materials, and it is assumed that for ferroelectricity and polarization, hydrogen bonding was crucial. In 1935, the first ferroelectric crystals were produced such as potassium dihydrogen phosphate (KDP) and ammonium salts ($NH_4H_2PO_4$, abbreviated as ADP). After finding KDP, there were no discoveries in a decade.(Lines and Glass 2001)

During and after the World War II, Barium Titanate which has a perovskite structure named after Count Lev Alekseevich von Perovskiy who is a Russian statesman and a minerologist(De Graef and McHenry 2007) was discovered in several countries such as United States, Russia, and Japan. In the USA, the research was accelerated. They produced ceramics by doping titanium dioxide with barium oxide (TiO_2 and BaO) with high dielectric permittivities in 1941. In 1945 and 1946, von Hippel in USA and Goldman and Wul in Russia experimented ferroelectric switching in the $BaTiO_3$ ceramic. They showed that hydrogen bonding was not necessary for ferroelectricity. After 1945, the works related with $BaTiO_3$ were accelerated. In 1949, Kay and Vousden discovered ferroelectric phase transitions which include tetragonal, orthorhombic, and rhombohedral

transitions. In 1952, Shirane and Hoshino discovered lead zirconate titanate (PZT), the best-known ferroelectric material. Since then, PZT is dominating the industry. Before 1984, because of high cost of producing single crystal, bulk ceramics were the main materials. In 1984, thin film ferroelectrics were developed, and researchers successfully integrated them into semiconductor chips.(Scott 2007)

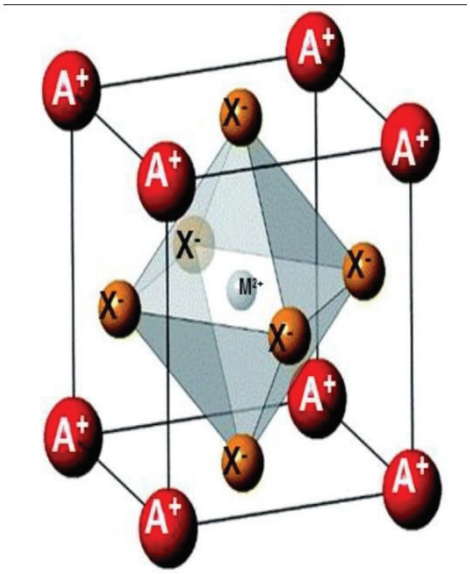

Figure 1.4. Structural representation of a perovskite material.(Katz 2020)

For environmental concerns, nowadays, scientists are trying to replace PZT with lead-free ceramics. Materials like sodium bismuth titanate (NBT)(Nakashima et al. 2007) and potassium sodium niobate (KNN)(Yin et al. 2018) have promising features. One of the newest examples to improve ferroelectric and piezoelectric properties is precipitation hardening. Zheng and coworkers successfully produced bulk ferroelectric materials with high piezoelectric properties.(M. Zheng, Zhao, and Rödel 2023)

1.2.3. Properties

To understand ferroelectrics, a bigger picture must be seen as Figure 1.5. illustrates. In general, in dielectrics, electric polarization can be induced under an external electric field.

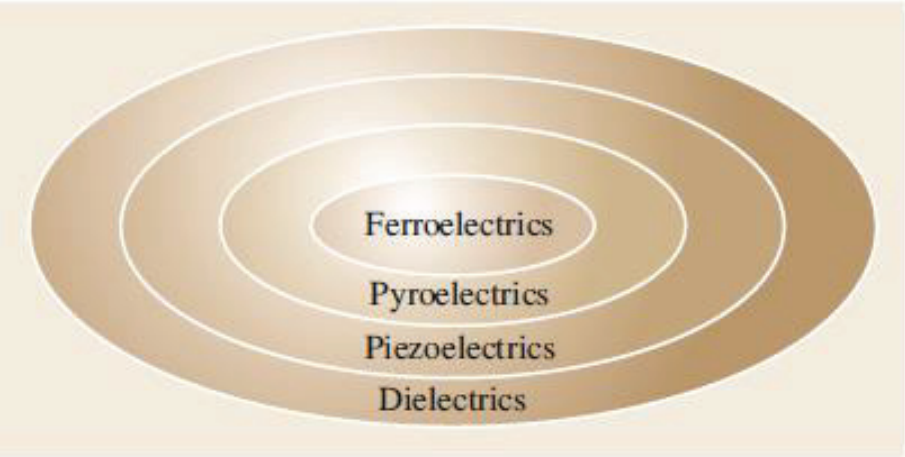

Figure 1.5. Schematic diagram of classification of dielectrics.(Whatmore 2017)

Crystal structures of electroceramics are categorized in two groups as centrosymmetric and noncentrosymmetric. Materials with noncentrosymmetric point groups allow piezoelectric effect. Noncentrosymmetrics, are further grouped in two: polar and nonpolar. Materials with Polar point groups allow spontaneous polarization and they can be pyroelectric or ferroelectric depending on whether the spontaneous polarization is switchable or not.(Pandey 2019)

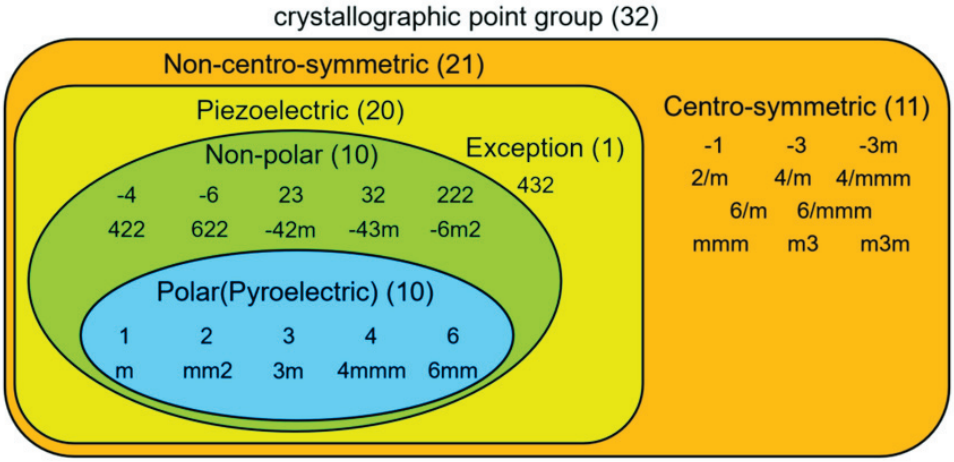

Figure 1.6. Crystallographic point groups.(Park et al. 2023)

There are three distinct forms of polarization: electronic, ionic, and orientation, commonly observed in dielectric materials based on the specific characteristics of the material and the mode of external field application. Electronic polarization results from the displacement of the centre of the negatively charged electron cloud in relation to the positive nucleus of an atom induced by an electric field (Figure 1.7a). Ionic polarization is exclusive to materials with an ionic nature, where an applied field acts the displacement of cations in one direction and anions in the opposite direction, resulting in the establishment of a net dipole moment (Figure 1.7b). Orientation polarization is identified in substances possessing permanent moments oriented in the direction of the applied field (Figure 1.7c). This alignment tendency, however, is counteracted with thermal vibrations of the atoms, leading to a reduction in polarization as temperature increases.(Callister and Rethwisch 2014)

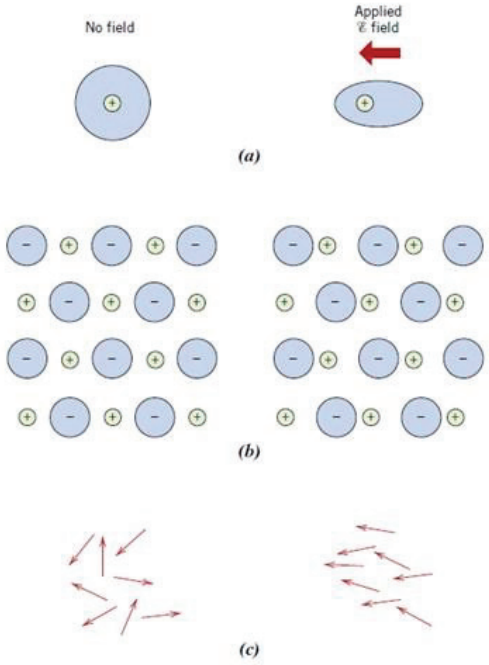

Figure 1.7. a) electronic polarization, b) Ionic polarization, c) Orientation polarization.(Callister and Rethwisch 2014)

In $BaTiO_3$, the spontaneous polarization is the result of the positions of Ba^{2+}, Ti^{4+} and O^{2-} ions within the unit cell (Figure1.8a). Barium ions located at the corners of the unit cell. This is the tetragonal symmetry. Relative displacements of Titanium and oxygen ions from their symmetrical positions cause the dipole moment. The O^{2-} ions are located slightly below, each of the six faces' centers, whereas the Ti^{4+} ion is displaced upward from the center (Figure 1.8b). This is called permanent orientation polarization. When the $BaTiO_3$ is heated above its Curie temperature (120 ^{o}C), the unit cell transformed into a cubic unit cell and lost its ferroelectric behaviour.(Callister and Rethwisch 2014)

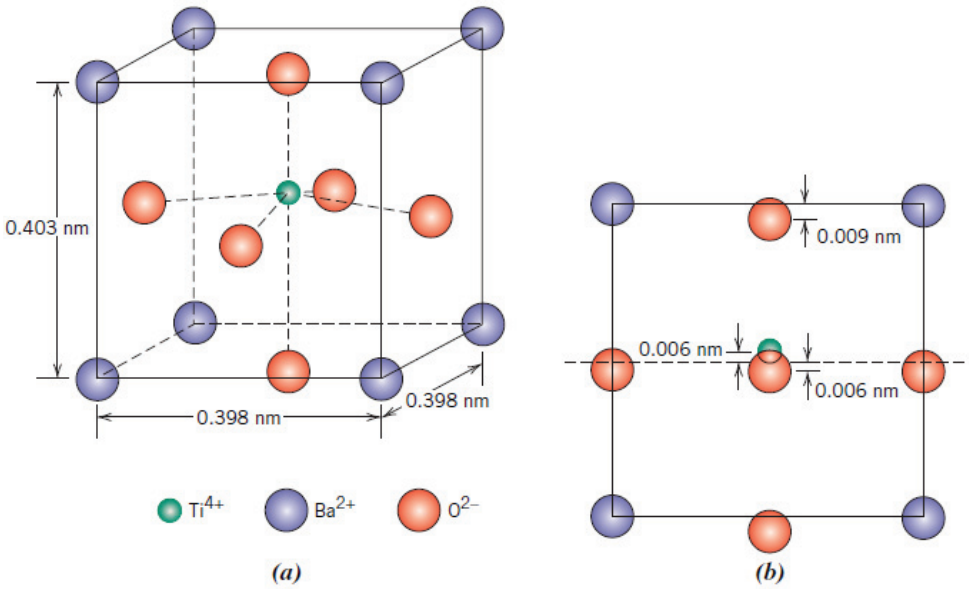

Figure 1.8. a) $BaTiO_3$ unit cell and b) one face of the unit cell of $BaTiO_3$, showing the displacements of Ti^{4+} and O^{2-} ions from center of the face.(Callister and Rethwisch 2014)

In general, direction of the polarization is not the same throughout the entire crystal. There are regions polarized in different directions. These regions are called domains. Domain walls are the boundaries between these regions. In the presence of electric field, it is possible to augment both the quantity and size of domains polarized in the direction of the external field. This procedure results in hysteresis in the P versus E curves upon the reversal of the field direction, consequently generating dielectric losses.(Dekker 1981) A visual example of domains can be seen in Figure 1.9.

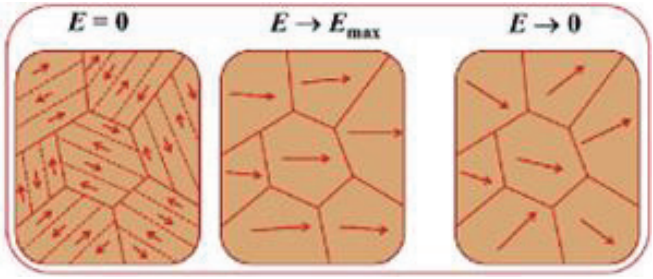

Figure 1.9. Alignment of ferroelectric domains in the presence of external electric field.(Nguyen et al. 2019)

With referring to Figure 1.10, let us consider a crystalline structure initially possessing a net zero polarization upon the application of an electric field to the crystal. The domain which is aligned of the same direction with electric field grow and polarization increases (OA). At the certain electric field values, all domains are aligned with the applied field direction (BC). In this case, polarization becomes saturated and theoretically, crystal consist of a single domain. The polarization is now called saturation polarization or maximum polarization. When the BC line is extrapolated to zero electric field, the polarization is called the spontaneous polarization, Ps. The electric field is reduced from point B to zero electric field and there remains the remnant polarization, P_r, at the zero electric field. Opposite direction of electric field must be applied to remove the remnant polarization so that the polarization of half the crystal to be reversed. The required electric field to sustain a zero polarization is called the coercive field. Coercive electric field affects the domain switching.(Dekker 1981)

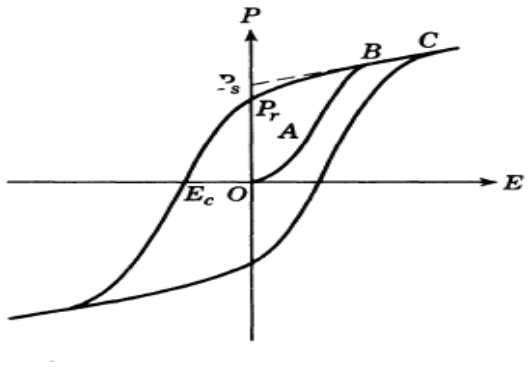

Figure 1.10. Representation of hysteresis loop in a polarization versus external electric field.(Dekker 1981)

The polar state is restricted to a limited temperature range for most ferroelectrics. A critical threshold is attained, when the temperature is increased, marking the transition from the ferroelectric (polar) phase to a nonferroelectric state, commonly referred to as paraelectric phase. A higher level of crystal symmetry is observed in paraelectric phase. The temperature at which this transformation occurs is denoted as the Curie temperature. This transition is a distinctive feature for most ferroelectrics but there are some exceptions like polymeric polyvinylidene fluoride (PVDF). It undergoes either melting or decomposition prior to reaching Curie temperature. For most ferroelectrics, the relative

permittivity is increased due to the approaching to Curie temperature, reaching a peak at that temperature and below it, permittivity is decreased. These ferroelectrics are called proper ferroelectrics. The other class of ferroelectrics called improper or extrinsic ferroelectrics. They show no peak in relative permittivity but an anomaly.(Whatmore 2017)

1.3. Electrocaloric Effect

1.3.1. Definition

In 2023, cooling systems still rely on vapor compression of gas refrigerants using greenhouse gases that are hazardous for environment.(Torelló and Defay 2022) Most of the refrigeration systems use hydrofluorocarbons as a refrigerant and 5% increase is expected for the next decade.(Sattar, Saidur, and Masjuki 2007) Solid state cooling is an alternative technology to the conventional cooling systems that use vapor compression.(Qin et al. 2022) It relies on caloric effects. Caloric effect refers to the reversible thermal changes observed in materials that are magnetically, electrically, and mechanically responsive when subjected to the proper applied fields. These thermal changes are assessed by measuring parameters such as adiabatic temperature change, isothermal heat and isothermal entropy change in terms of ΔT, Q and, ΔS respectively.(Barman, Kar-Narayan, and Mukherjee 2019) ΔT is the adiabatic temperature change occurred in response to a change in external electric field.(Correia and Zhang 2014) $\Delta T/\Delta E$ is another important parameter that measures the amount of adiabatic temperature change (ΔT) obtained per applied electric field, which is sometimes called electrocaloric efficiency or electrocaloric strength.(Karakaya 2022)

The materials which exhibit caloric effects are called caloric materials. Depending on applied field, materials are classified as magnetocaloric (MC), electrocaloric (EC), mechanocaloric (mC) and mechanocaloric are also divided into two groups: elastocaloric (eC) and barocaloric (bC). When they develop temperature difference in response to a magnetic field; they are called magnetocaloric, when they respond to an electric field, they are called electrocaloric and if there respond to a mechanical stress (for elastocaloric, it is a uniaxial stress and for barocaloric, it is a hydrostatic pressure), it is called

mechanocaloric.(Torelló and Defay 2022) The coefficient of performance (COP) in cooling systems quantifies the heat removal efficiency per unit of electrical energy consumed.(Qin et al. 2022) The conventional cooling systems have relatively low COP values. For air conditioning units, COP is between 2.7 and 4.2. For refrigerators, COP values are between 0.71 and 1.6. The novel solid state refrigeration technologies, namely magnetocaloric with a COP of 7, elastocaloric with a COP of 11,8 and electrocaloric with a highest 13 exhibit a significantly higher coefficient of performance compared to traditional technologies.(Ma et al. 2017) Table 1.1 shows the comparison of COP values of conventional and novel materials. Due to their high-energy density and inherent compatibility with their circuitry, electrocaloric materials are favourable choice for portable, compact cooling applications, even though they operate at temperatures different from the ambient temperatures.(Cazorla 2019) EC utilizes electricity directly and compared to other caloric materials, it has a high energy efficiency.(Torelló and Defay 2022)

Table 1.1. Comparison of COP values of conventional and novel systems

Type	**Coefficient of Performance**	**Reference**
Conventional (Air Conditioner)	3.6 – 4.2	(Hannun and Hamza 2021)
Conventional (Air Conditioner)	2.7- 3.6	(“Understanding How Efficient Your Air Conditioner Is,” n.d.)
Conventional (Refrigerator)	0.71-1.16	(Staley, Bullard, and Crawford 1992)
Magnetocaloric	7	(Dall’Olio et al. 2021)
Mechanocaloric	11.8	(Cui et al. 2012)
Electrocaloric	13	(Ma et al. 2017)

For electrocaloric materials, efficiency of energy conversion is as high as magnetocaloric materials, around 60-70% while conventional fridges have approximately 40-50% efficiency.(Correia and Zhang 2014) Electrocaloric materials emit no harmful gas directly such as gases with ozone depletion potential and/or global warming potential.(Shi et al. 2019)

1.3.2. History

The first discovery was in 1878 when electrocaloric phenomena were introduced as the converse effect of pyroelectricity by William Thomson, Lord Kelvin.(Correia and Zhang 2014) In 1930, half a century after Thomson's work, electrocaloric effect made its debut, observed in Rochelle Salt, and precisely quantified by Hautzenlaubin in 1943. The year 1946 marked the discovery of ferroelectricity in barium titanate ($BaTiO_3$), a perovskite and numerous other perovskite oxides such as $LiNbO_3$, $LiTaO_3$, $KTaO_3$, $KNbO_3$, $PbTiO_3$. In the early 1950s, the family of solid solutions of PZT was identified as a novel ceramic material. As the 1950s ended, the pyroelectric effect, the converse of the electrocaloric effect in perovskite oxides, began finding wide applications, especially as sensors. While perovskite oxides were dominant in the fields of ferroelectrics, research on the electrocaloric effects in these materials remained limited. It wasn't until 1961 that a new class of relaxor ferroelectric materials were uncovered in the perovskite oxide $PbMg_{1/2}Nb_{1/2}O_3$ (PMN), offering promising potential for electrocaloric cooling applications. In 1962, maximum electrocaloric properties of barium titanate was found by Karchevskii with $\Delta T = 1.8\ K$. This high value was found at the phase transition. In 1968, in various doped and undoped $PbZr_xTi_{1-x}O_3$ (PZT) materials, ΔT was found 1.6 K.(Barman, Kar-Narayan, and Mukherjee 2019) Ragdebaugh developed and tested the first cryogenic electrocaloric refrigerator concept in 1977. He used materials with low phase transition temperature such as $SrTiO_3$ and $KTaO_3$.(Radebaugh et al. 1979) Shebanov and Borman measured electrocaloric effect of lead scandium tantalate ($PbSc_{0.5}Ta_{0.5}O_3$) in 1992.(Shebanov and Borman 1992) In the initial decades following the discovery of the electrocaloric effect in solid materials, only a handful of research teams focused on advancing electrocaloric refrigeration. This was primarily because the electrocaloric effect in bulk materials was found to be relatively small. However, the perception of electrocaloric materials underwent a significant change in 2006 when a high electrocaloric temperature change of 12 K was indirectly observed in thin films close to paraelectric phase transition at 225 ^oC by Mischenko and colleagues.(Mischenko, Zhang, Scott, et al. 2006) After 2 years later, electrocaloric effect with ΔT of 12 ^oC found in polyvinylidene fluoride trifluoroethylene [P(VDF-TrFE)] thin films at 70 ^oC by Neese and coworkers.(Neese et al. 2008) In 2013, another giant electrocaloric effect of Ba-doped $PbZrO_3$ thin films with $\Delta T = 45.3\ K$ was reported by Peng.(Peng, Fan, and Zhang 2013)

Since 1960, fewer than 270 scientific papers have been published on this subject and more than 65% of these papers were published in the last decade, showing a substantial increase in research activity and progress from 2006 onwards.

1.3.3. Working Principle and Thermodynamic Approaches

The fundamental operational principles of electrocaloric refrigeration bear a resemblance, in principle, to those of magnetic and gas compression cooling. They involve the transfer of heat from a heat source to the surrounding environment through a working body (which can be an electrocaloric material or gas) subjected to a thermodynamic cycle. Refrigeration cycles rely on changes in entropy within the working body (or refrigerant), while an electric field varies (pressure in the vapor-compression cooling).(Correia and Zhang 2014) There are several definitions in thermodynamics which will be mentioned in this topic. Adiabatic process is a process which there is no heat transfer. Isothermal process is that the temperature is constant during the thermodynamic process and isofield process is like the isothermal, but an external field (magnetic or electrical) is constant. There are three common thermodynamic refrigeration cycles which are Carnot, Brayton, and Ericsson cycles. Of these, the Brayton cycle is the easiest one to put into practice, characterized by two adiabatic and two isothermal steps, while Ericsson cycles mainly differ from Brayton cycles in their application or removal of an external stimulus in the isothermal steps.(Correia and Zhang 2014)

For Brayton cycle, in the first step (A-B in Fig 1.11a and 1-2 in Fig 1.11b), electric field is applied in a shorter time scale than the thermal relaxation time constant of the system adiabatically. After that, temperature is increased. In the second step (B-C in Fig 1.11a and 2-3 in Fig 1.11b), the electric field is kept constant for a certain time. Material releases heat to the surroundings. After that, electric field is removed adiabatically (C-D in Fig 1.11a and 3-4 in Fig 1.11b), and EC temperature is decreased. At E=0, the material absorbs heat from surroundings and the initial state is achieved (D-A in Fig 1.11a and 4-1 in Fig 1.11b).

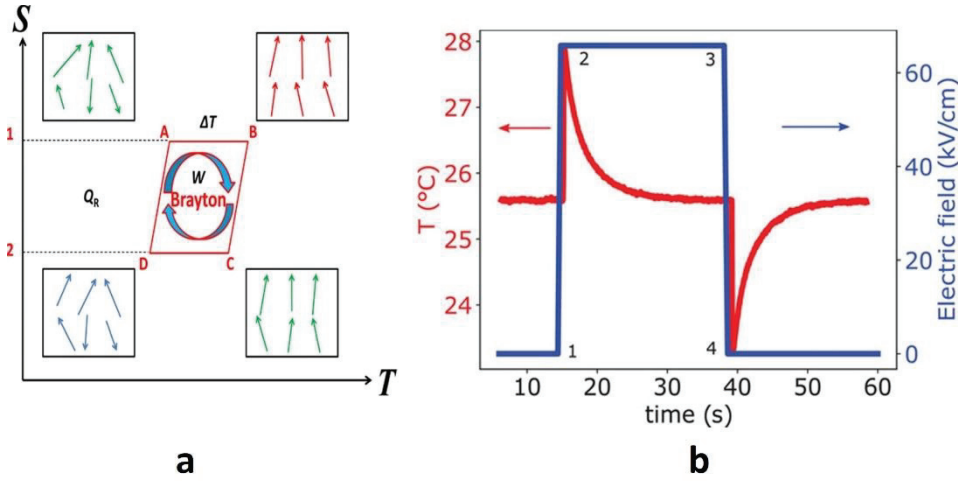

Figure 1.11. Brayton cycle in terms of a) entropy versus temperature and b) temperature and electric field versus time.(Liu, Scott, and Dkhil 2016)·(Torelló and Defay 2022)

1.3.4. Measurement Methods

There are two primary approaches to measuring the electrocaloric effect in terms of temperature change: the direct method and the indirect method. In the direct method, several measurement techniques are employed, including the utilization of thermocouples or thermometers, specially designed calorimeters, infrared (IR) cameras, and scanning thermal microscopy. At first, the direct approach to measurement may appear to offer greater confidence when it comes to the design of electrocaloric devices. Nevertheless, practical scenarios introduce various complexities that hinder the achieving of perfectly adiabatic conditions. Notably, the crucial factor in direct measurements lies in proper thermal isolation of the sample. It is essential to bear in mind that all measurement cycles assume perfectly adiabatic conditions. However, the reality of practical situations involves the constant presence of thermal exchanges between the electrocaloric materials and their surrounding environment. This continuous thermal interaction results in a characteristic exponential decay of the electrocaloric peak as measurement time progresses. It is under such circumstances that indirect measurement techniques become useful. In addition, the indirect measurement is preferred due to its practicality compared to direct measurement methods.

For the indirect measurement, let's investigate the basic thermodynamic relations. Maxwell relations can be useful to measure electrocaloric temperature change ΔT. These relations are,

$$\left(\frac{\partial S}{\partial E}\right)_T = \left(\frac{\partial P}{\partial T}\right)_E \tag{1.2}$$

Based on these relations, the reversible electrocaloric change in temperature ΔT of a material that is electrically responsive due to the change in applied electric field $\Delta E = E_2 - E_1$ under adiabatic conditions can be determined by

$$\Delta T = -\int_{E_1}^{E_2} \frac{T}{C(E,T)_\rho}\left(\frac{\partial P}{\partial T}\right)_E dE \tag{1.3}$$

where T is the temperature, ρ is the density, P is the polarization and C (E, T) is the heat capacity and they all depend on electric field and temperature. Given our knowledge of parameter P (E, T), the process simplifies into a mathematical problem, encompassing the calculation of its derivatives and integrals, consequently leading to the determination of ΔT. In experimental settings, the choice often favours the upper branches of P loops (specifically the one called as second quadrant), where the electric field E is greater than zero. This selection ensures the reliability of the indirect method, which relies on Maxwell relations. In contrast, lower branches (E) loops (E>0) pose challenges due to the lower electric field threshold, leading to undesired ferroelectric switch€. P(E) loops are measured at a constant temperature and at different temperature when the sample is heated. It's essential to maintain sufficiently small temperature intervals to achieve smooth isothermal P-T curves.(Liu, Scott, and Dkhil 2016)

1.3.5. Materials

To observe electrocaloric (EC) effects, it is essential to apply a voltage difference between adjacent electrode plates containing the EC material. Typically, there are three distinct configurations for these electrode plates as illustrated in Figure 1.12: bulk, thin films, and multilayer capacitors. Bulk structures involve large, flat samples with

electrodes positioned on the top and bottom surfaces. These electrodes can effectively cover most of the sample's surface, resulting in a nearly 100% electrocaloric active sample. This configuration is convenient and suitable for practical device integration. However, it comes with the drawback of having a significant distance between the electrodes, requiring high voltages, which can present challenges in terms of experimental setup and safety. One solution to reduce the required voltage is the utilization of thin films. Thin films are ultra-thin layers of EC material) grown on a substrate. Due to their low thickness, they can generate much higher electric fields at relatively low applied voltages, leading to high EC effects. Nevertheless, the handling of thin films can be intricate and impractical, making them less viable for applications involving the continuous cooling of macroscopic objects. The third option is multilayer capacitors (MLCs). MLCs adopt an engineered-like structure comprising thick EC films stacked with electrodes piled up between them. These electrode sheets are connected in parallel through electrical terminals, typically situated on the sides of the structure.(Torelló and Defay 2022)

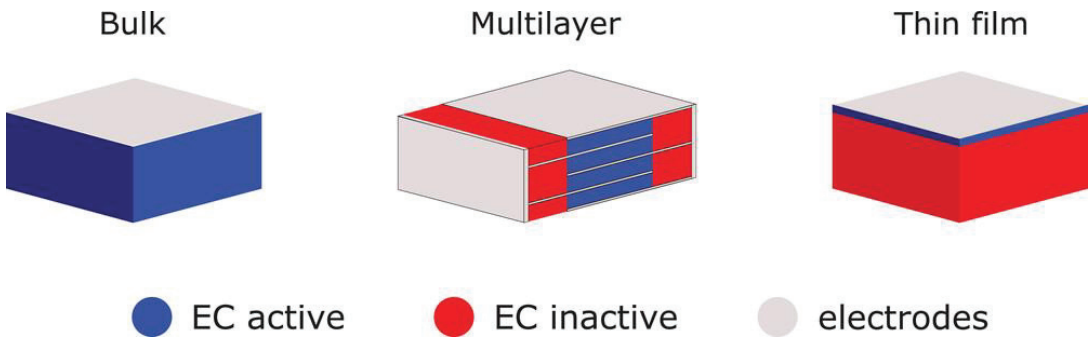

Figure 1.12. Graphical representation of the bulk, multilayer capacitor, and thin film structures.(Torelló and Defay 2022)

Electrocaloric properties are directly related with ferroelectric properties so the literature usually corelates with developments in ferroelectric materials. In ferroelectric, piezoelectric and electrocaloric research, two systems, lead-containing and lead-free are investigated. Both Pb-containing and Pb-free ferroelectric materials can be classified according to their transition behaviour from ferroelectric to non-ferroelectric phase. To state differences between their physical and thermal behaviour, phase transitions such as first order and second order phase transitions and relaxor phase transition are important

key factors. In both first order and second order transitions, frequency dependence of dielectric constant is weak. First order phase transition as illustrated in Fig 1.14a involves latent heat at a specific temperature. This latent heat is a characteristic discontinuity and is called Curie point. After this point, material becomes paraelectric. Another determining evidence of the first order phase transition is double hysteresis loops as illustrated in Figure 1.13. A strong electric field is applied to the material a few degrees above its transition temperature. When the electric field is zero, the material becomes non-ferroelectric but at a certain value of the external electric field, the polarization increases dramatically and upon reversal of the electric field, hysteresis observed. At low electric fields, the behaviour becomes normal again. Second order phase transition as shown in Figure 1.14b, on the other hand, is a continuous phase transition. There are large fluctuations of polarization before the transition which acts as a warning. The spontaneous polarization should obey the $T^{1/2}$ relationship. In this transition, the Curie point is where the polarization becomes zero and material becomes paraelectric. Relaxor ferroelectrics are different than ferroelectric with first and second order phase transitions due to their strong frequency dependent dielectric constant. Their structures are usually perovskites. The transition from ferroelectric to paraelectric phase is dependent on both temperature and frequency when measuring dielectric constant. They also show hysteresis loops of polarization, but these loops are narrow.(Pandey 2019)

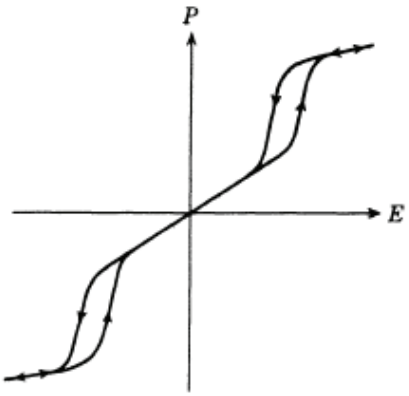

Figure 1.13. Schematic representation of a double hysteresis loop.

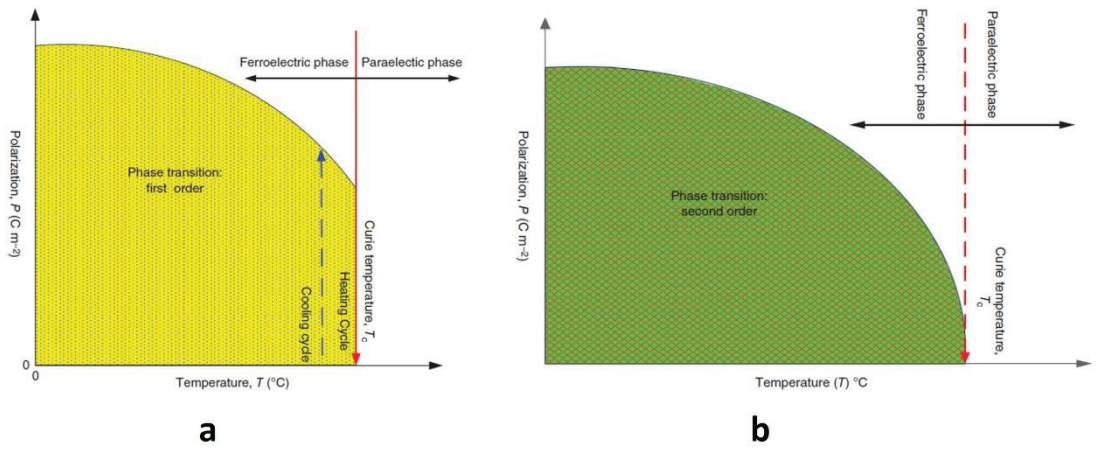

Figure 1.14. a) First order phase transition and b) second order phase transition in polarization - temperature relationship.(Pandey 2019)

1.3.5.1. Lead-based Materials

Lead-containing systems are perovskite structures with Pb as at the A-site. Lead is used with dopants usually. Lead zirconium titanate (PZT) is the most frequently used material in the industry as a transducer or sensor. Suchanicz and coworkers showed that the PZT has a dielectric thermal hysteresis. For nearly seventy years, PZT has dominated the industry and in the last decade, there were several findings. Suchanicz and coworkers showed that PZT ceramic has a thermal hysteresis in dielectric permittivity on the absence of pressure. Thermal hysteresis in the dielectric permittivity is one of the characteristic features of the first order phase transition. When pressure is increased, (up to 1000 bar) hysteresis is reduced; suggesting that the first order transition becomes second order transition.(Suchanicz et al. 2008) There are other lead-based materials with different dopants and compositions. Lead-titanate ($PbTiO_3$) is one of these materials as illustrated in Figure 1.15. Binary system is obtained with sodium bismuth titanate (NBT). High dielectric constant was observed, and thermal hysteresis of dielectric permittivity was also seen in PT-NBT system which proves the first-order phase transition. Curie temperature was lower than PT and higher than NBT systems.(Czaja et al. 2020) Chu and colleagues worked on lead scandium niobate. Double loop of ferroelectric hysteresis around the Curie temperature, heat flow hysteresis and dielectric thermal hysteresis were shown as characteristic features of first-order transition. According to work, A-site

vacancies strongly affect dielectric and other properties.(Chu, Reaney, and Setter 1995) Among lead-based relaxors, lead magnoniobate, $PbMg_{1/3}Nb_{2/3}O_3$ (PMN) is the most prominent system. Both real and imaginary parts of the dielectric constant were strongly dependent on frequency, showing the relaxor ferroelectric characteristics.(Kirillov and Isupov 1973)

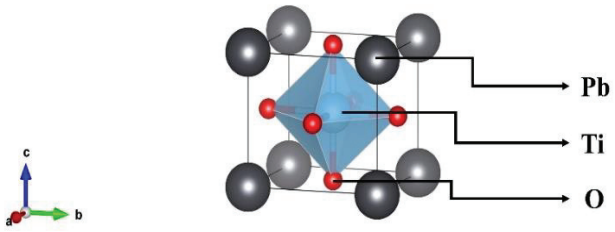

Figure 1.15. Crystal Structure of PT

Correlated with ferroelectric properties, electrocaloric properties were also favourable in lead-based materials. For PZT thin films, Mischenko and coworkers found that a giant ΔT of 12 K, with wide operating temperature range but, also with a high Curie temperature of 222 ºC.(Mischenko, Zhang, Scott, et al. 2006) Same research team also found that PMN-PT thin film relaxor ferroelectric with ΔT of 0.9 K near room temperature and ΔT of 5 K at 75 ºC. A broad temperature range with relatively large ΔT was observed. It was promising that the relaxor behaviour can contribute to the electrocaloric properties.(Mischenko, Zhang, Whatmore, et al. 2006) There were other reports such as $Pb(Zr,Sn,Ti)O_3$ system with ΔT of 2.6 K, 161 ºC of Curie point and a wider temperature range of 21 ºC.(Tuttle and Payne 1981) and lead scandium tantalate (PST) with ΔT of 3.7 K and a narrow temperature range. PST system also exhibits thermal hysteresis on dielectric constant as a proof of first-order phase transition.(Nouchokgwe et al. 2021) Lead is an important element for ferroelectric, piezoelectric and electrocaloric properties. The reason behind this importance lies in lead's electron structure. In solid-state materials, the presence of lone pairs has usually been linked with Pb. These lone pairs are formed by the Pb atom's $6s^2$ electrons, which occupy an orbital generated

through the hybridization of the 6s and 6p atomic orbitals. These chemically inert electrons are believed to exert steric influence, leading to the distortion of crystal structures which is important for polarization of the structure.(Walsh and Watson 2005) However, lead is a toxic element which contaminate the environment, but has relatively low cost as illustrated in the Figure 1.16. Waste electrical and electronic equipment amount in the world is on a significant upward trajectory.(Rödel et al. 2009) European Union changed the directive of "Restriction of Hazardous Substances (RoHS)" in 2015. EU included some substances such as lead, mercury, cadmium.(Directive 2013) As alternatives, lead-free materials come into play such as barium titanate, sodium bismuth titanate, potassium sodium niobate and so on.

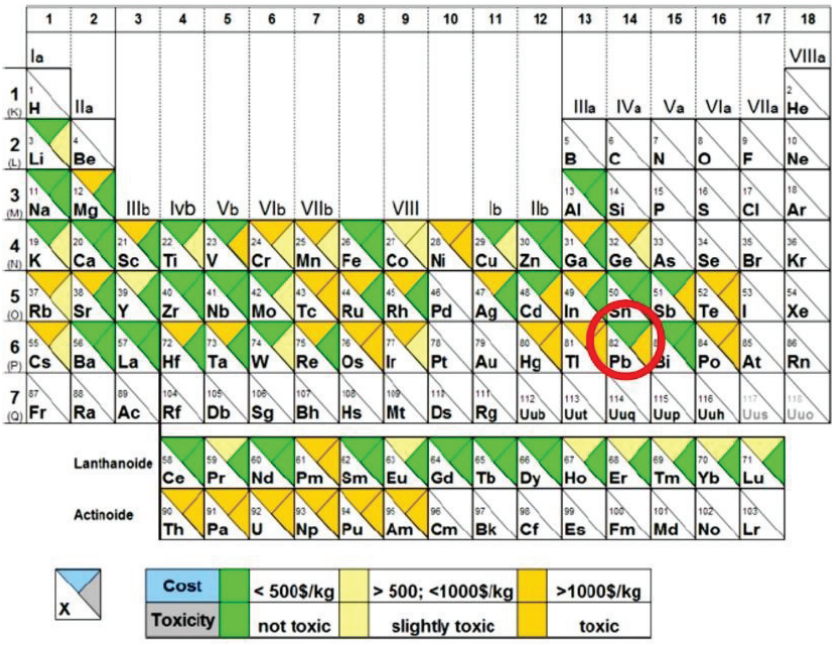

Figure 1.16. Comparison of elements in terms of toxicity and cost in the periodic table.(Rödel et al. 2009)

1.3.5.2.Lead-free Materials

As lead-based materials, most of the lead-free materials also have perovskite structure. Among these materials barium titanate, $BaTiO_3$ (BT) is the most important electroceramic material. After the discovery in 1940s, BT became at the centre of research area. The Curie point is found about 123 ^oC.(Sakayori et al. 1995) Merz observed that

double hysteresis loop near Curie point of BT.(Merz 1953) Research showed that the BT has a first-order phase transition. BT is mostly used with other dopants and systems such as zirconium (Zr), strontium (Sr) and so on. By adding Zr at the B-site,in $Ba(Zr,Ti)O_3$ system, first-order phase transition becomes second-order. Curie point is lowered when Zr amount is increased, and dielectric maxima peaks are broadened as illustrated in Figure 1.17.(Hennings, Schnell, and Simon 1982) Like Zr, Sr substitution at the A-site also causes transformation of phase transition from first order phase transition to diffuse phase transition but this transformation is not significant compared to Zr-doping. Sr.(Bai, Han, Ding, et al. 2013) Single crystal BT has also good electrocaloric properties. Bai and coworkers found a ΔT of 4.8 K at the temperature that is a bit higher than the phase transition temperature.(Bai, Han, Zheng, et al. 2013) Zr affects the electrocaloric properties. By increasing the amount of Zr, ΔT is decreased but operating temperature range is enhanced due to the broadened phase transition.(Jian et al. 2018) Qian and colleagues also worked on Zr doping of BT by using solid state reaction method. They found much higher ΔT of 4.5 K in a broad temperature range of >30 °C.(Qian et al. 2014)

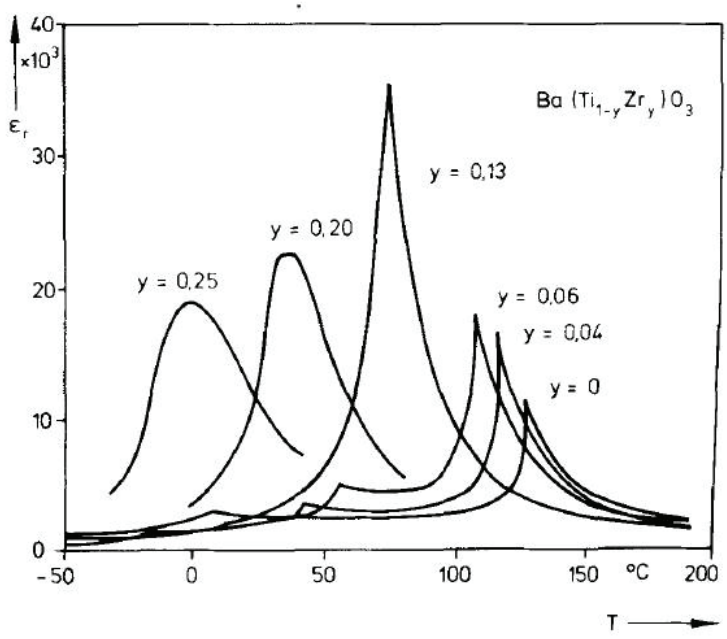

Figure 1.17. Temperature dependence of permittivity of ceramic $BaZrTiO_3$.(Hennings, Schnell, and Simon 1982)

Sodium bismuth titanate (NBT) system is another lead-free system. Just like lead, bismuth has also lone electron pair which might contribute to the ferroelectric and electrocaloric properties. Unlike BT, NBT is a relaxor ferroelectric. It shows typical

features of relaxors such as a broad peak and frequency dependent of dielectric constant as shown in Figure 1.18.(Shvartsman and Lupascu 2012)

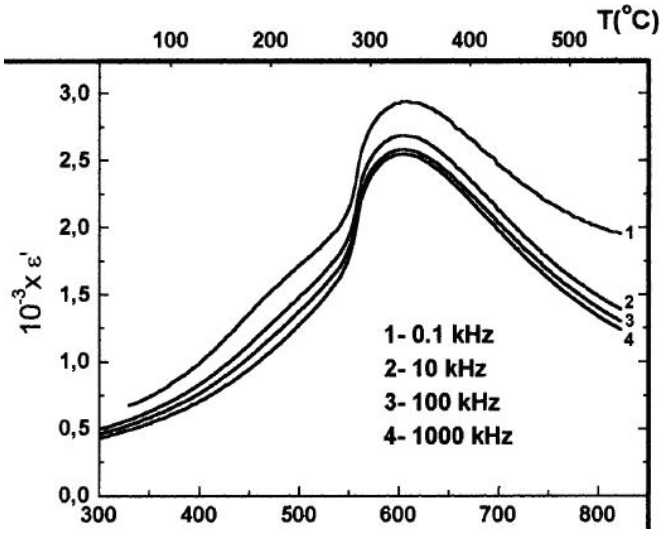

Figure 1.18. Temperature dependence of the dielectric constant at different frequencies for NBT system.(Shvartsman and Lupascu 2012)

BT and NBT can also be used as a solid solution BT-NBT. This system is still open to debate there are uncertainties about phase transitions and ferroelectric properties. Increasing NBT content enhances the dielectric properties and increases the Curie temperature up to 180 °C.(Yoon, Kim, and Kim 2017) As expected, broad peak in dielectric constant is enhanced as NBT amount is increased as illustrated in Figure 1.19.(Gomah-Pettry et al. 2004) BT-NBT system is a promising system for electrocaloric properties with ΔT of up to 2.1 K.(X.-C. Zheng et al. 2012) Availability of these components is another issue that should be considered. At the end, to use these systems in the applications, cost and availability become crucial factors. Zirconium as a dopant element for electroceramic systems is more than nearly three times as abundant as copper and ten times more abundant than lead. 165 parts/million by weight lay in earth's crust.(Chemicool.com 2012) Australia and Southeast Asia regions have the highest market of zirconium.(Mordor Intelligence Research & Advisory 2023) Zirconia (ZrO_2), raw mineral for electroceramic synthesis, also has a huge market in Southeast Asia, especially in India and China. Market size and its derivatives will grow continuously.(Kiran Pulidindi 2023) These statistics show that zirconium is a suitable chemical for widespread applications for future.

For a typical barium titanate – sodium bismuth titanate, availability of raw components are also high. Bismuth and titanium have high market concentration in worldwide. Asia and Pacific region are the dominant supplier in the world. Sodium market is expected to grow in future and besides bismuth, titanium and zirconium, Asia and Pacific region is the main supplier region. For barium, market concentration is low but besides Asia and Pacific region, Turkey is one of the countries that has a source of barite ore.("Barit," n.d.)·("Global Sodium Carbonate Market" 2022)·("Titanium Market Size & Share Analysis - Growth Trends & Forecasts (2023 - 2028)," n.d.)·("Bismuth Market - Growth, Trends, COVID-19 Impact, and Forecasts (2023 - 2028)," n.d.)

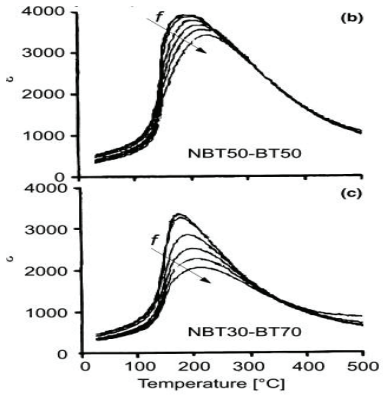

Figure 1.19. Temperature dependences of the dielectric constant at different frequencies for NBT50-BT50 (top) and NBT30-BT70 (bottom).(Shvartsman and Lupascu 2012)

1.4.Motivation of the Thesis

Electrocaloric properties of BT is studied extensively in the past and today. As a single crystal(Bai, Han, Zheng, et al. 2013) or polycrystalline(Karchevskii 1962a), ΔT values were significantly higher but operating temperature ranges were relatively low. Zr doping of BT, on the other hand, increases ΔT and temperature range. Qian and coworkers studied BT ceramics with Zr doping. ΔT is found that 4. 5 K and temperature range is larger than 30 ^{o}C for 0.2 mol Zr in $BaZr_xTi_{1-x}O_3$ at high electric fields. This result shows that Zr doping would increase both ΔT and temperature range (nearly eleven folds of ΔT of Zr doped BT compared to pure BT)(Qian et al. 2014) Jian and colleagues also worked on Zr-doped BT system. They measured ΔT of 2.4 K for $BaZr_{0.05}Ti_{0.95}O_3$. However,

increasing Zr content to 0.30 mol decreased the electrocaloric properties (ΔT of 1.24 K) as well as polarization and ferroelectric properties. Crystal structure is another parameter for electrocaloric and ferroelectric properties. It is shown that just like lead doping into BT system, NBT doping also increases the tetragonality in BT systems dramatically. Enhancement of tetragonality may also affect the order of the phase transition and it may be one of the key factors to improve electrocaloric and ferroelectric properties. Karakaya worked on BT-NBT systems. By using indirect method, high ΔT values are obtained as illustrated in Figure 1.20. Dr. Lovro Fulanovic also measured the ΔT values by using direct method for (1-x)BT-xNBT where x= 0.1 and 0.2 as shown in Figure 1.21. Results of direct method are close to indirect method measurements which shows the high reliability of measurements of indirect method.(Karakaya 2022)

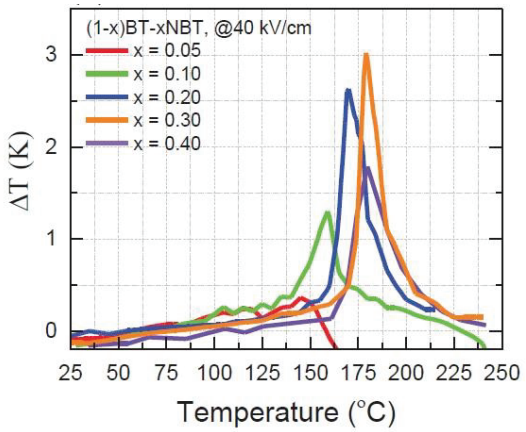

Figure 1.20. Comparison of temperature dependent ΔT values of (1-x)BT-xNBT by indirect method.(Karakaya 2022)

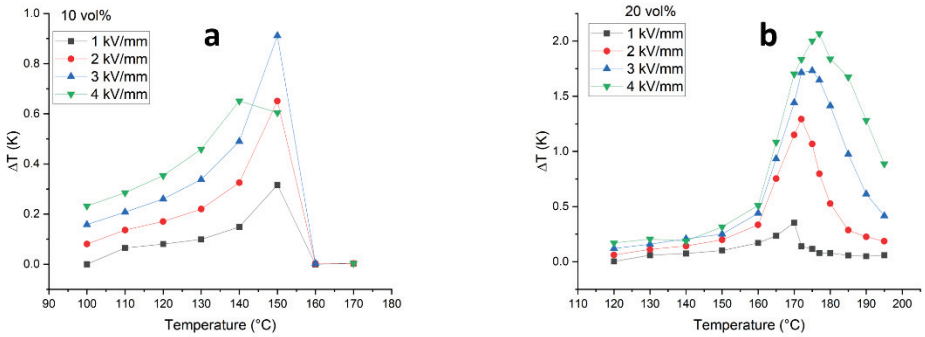

Figure 1.21. Temperature dependent ΔT values of (1-x)BT-xNBT where x= a) 0.1 and b)0.2 by direct method.

The aim and the motivation of this thesis are to synthesize BT-NBT system with Zr doping, measuring dielectric, ferroelectric and finally, electrocaloric properties, obtaining large ΔT with a broad temperature range and investigating Zr influence of the dielectric, ferroelectric and electrocaloric properties on BT-NBT system. BT-NBT system with Zr-doped is arranged as $0.70(BaZrTiO_3)$-$0.30(Na_{0.5}Bi_{0.5}TiO_3)$ for $0 \leq x \leq 0.05$ mol. The other parameters such as calcination time and temperature and sintering time and temperature kept constant. Dielectric properties were measured at different frequencies between room temperature and 250 °C. Ferroelectric and field-induced strain properties were investigated at different temperatures (from 25 to 250 °C) and different electric fields. Finally, electrocaloric properties were analysed between 25 and 250 °C at different electric fields.

CHAPTER 2

EXPERIMENTAL METHODS

2.1. Material Preparation

This section provides a comprehensive explanation of the synthesis method of "Barium titanate- Bismuth Sodium Titanate with Zirconium substitution $Ba_{0.7}Na_{0.15}Bi_{0.15}Ti_xZr_{1-x}O_3$ where 0 =< x => 0,05)". Compositions are labelled as BxZT-NBT where x is the percent amount of Zr mol as shown in Table 2.1. Figure 2.1. illustrates the steps of the synthesis. BZT-NBT ceramics were prepared by using solid state reaction method. From raw powders, bulk ceramics are synthesized in a pellet form. Starting raw powders are barium carbonate ($BaCO_3$, > 99.8%), titanium dioxide (TiO_2, > 99.5%), sodium carbonate (Na_2CO_3, >99.8%), bismuth oxide (Bi_2O_3, >99.9%), and zirconium oxide (ZrO_2, >99%). First and foremost, the raw powders were dried to remove water molecules in a drying oven at 200 ºC overnight. Then, these powders are weighed according to previously calculated stoichiometric ratios. Subsequently, weighed powders are mixed with ethanol and yttrium-stabilized zirconia balls in a High-Density Polyethylene (HDPE) bottle and ball-milled in a planetary ball mill at 250 rotations per Minute (RPM) for 24 hours. After ball milling, the mixture was dried at 100 ºC for 30 minutes in a drying oven to remove ethanol from the mixture. Powders are pressed into pellets at 1.5 tonnes at a hydraulic press for a better solid-state reaction and calcined at 1025 ºC for 2 hours at a rate of 5 ºC/min. To prepare a mixture with the binder, calcined pellets were ground into powder. Poly-vinyl alcohol (PVA)-pure water solution is prepared by using magnetic stirrer at 750 RPM at 80 ºC to use %4wt PVA as a binder. After the preparing of PVA-pure water solution, pure water and %0.03 mol MnO_2 (to increase the resistivity) was added to mixture resistivity for better electrical measurements. Mixture is ball milled in the planetary ball mill at 250 RPM for 24 hours. The mixture was dried at 100 ºC for 30 minutes in the drying oven. Powder, then, was sieved by a 63 μm sieve. Final powders are pressed into pellets at 1.5 ton in the hydraulic

press. Finally, to burn-out PVA, pellets are heated tot 600 ºC for 4 hours at a rate of 1 ºC/min and sintered at 1200 ºC for 2 hours at a rate of 5 ºC/min. For microstructural analysis, pellets are polished by sandpaper and for electrical measurements, in addition to polishing, both surfaces of pellets are coated with silver paint as electrodes and the paint was cured at 200 ºC for 20 minutes in the drying oven.

Table 2.1. Labelling of compositions based on Zr doping.

Composition	**Amount of Zr doping (% mol)**
B0ZT-NBT	0
B1ZT-NBT	1
B2ZT-NBT	2
B3ZT-NBT	3
B3,5ZT-NBT	3,5
B4ZT-NBT	4
B5ZT-NBT	5

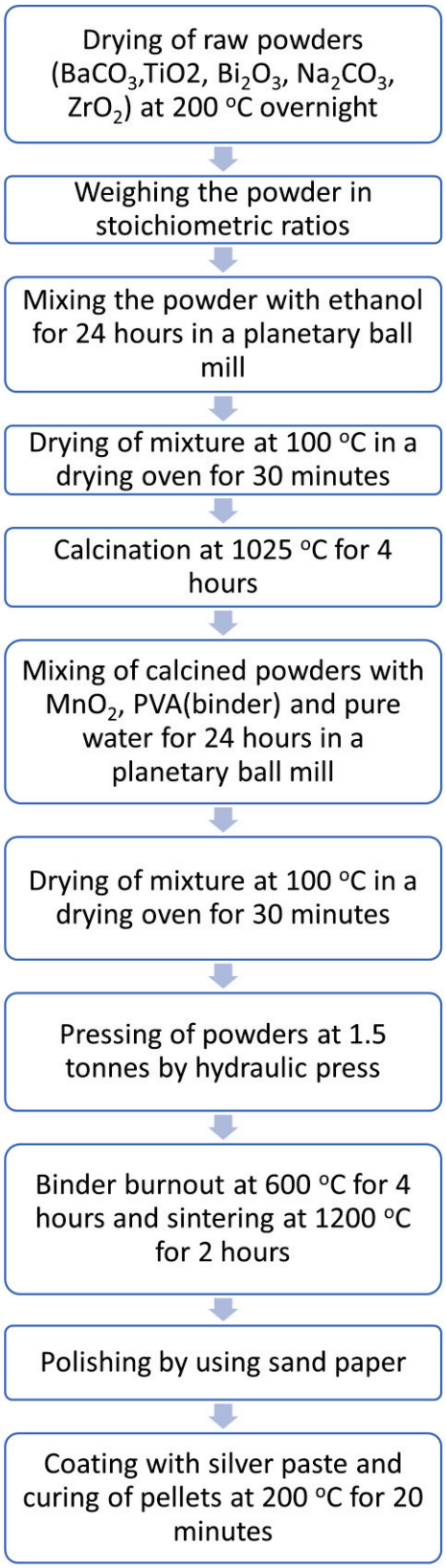

Figure 2.1. Flow chart of synthesis of $Ba_{0.7}Na_{0.15}Bi_{0.15}Ti_xZr_{1-x}O_3$ compositions.

2.2. Characterization Methods

2.2.1. Phase Analysis (XRD)

X-ray diffraction (XRD) technique is used to determine crystal structure and different phases in a crystallographic material. To obtain the information about incorporation of substituting atoms, XRD technique is a simple yet effective method.. For this work, XRD data is collected between 20-80 angles with 0.05 °/sec step time at Izmir Institute of Technology (IZTECH) Materials Research Center by using a high resolution X-ray diffractometer (Bruker D8). The phase analysis was done using HighScore Plus software.

2.2.2. Microstructure Analysis

Microstructural analysis (grain size, shape, impurity) is performed by a Scanning Electron Microscope (SEM). SEM uses a beam of electrons to create highly detailed images of samples. The images produced by SEM can reveal fine details such as grain size, shape, composition and other chemical and physical properties of a sample.(Goldstein et al. 2017) The SEM analysis was done using FEIQUANTA 250 FEG, IZTECH Material Research Center. Grain size analysis is done by using ImageJ software.

The basic working principle of the SEM is the generation of a focused beam of high energy electrons by emission from an electron source. After emission, the electron beam is modified by some advanced parts such as apertures, lenses, and coils. Modified electron beam scans the sample and from this interaction, two outgoing electrons are produced: 1- Backscattered electrons which emerges from the sample with a large portion of their incident energy remains still after exposing scattering. 2- Secondary electrons that escape the specimen surface after beam electrons have ejected them from the atoms in the sample. Secondary electrons are generally used for morphological and topographic analysis. To reveal multiphases, backscattered electrons are used to see the contrast. SEM also gives qualitative elemental analysis by using Energy Dispersive X-ray Spectrometry (EDX). A specific X-ray can only be created under certain conditions; The energy of the incident beam exceeds the critical ionization energy for the atomic shell. This ionization

leads to the emission of the characteristic X-rays which give elemental information.(Goldstein et al. 2017) For SEM analysis, sintered samples in a pellet form were polished by 1000 mesh SiC sandpaper. After polishing, thermal etching was done at 1100 ^{o}C for 2 hours at the heating/cooling rate of 5 ^{o}C/min. Polishing and thermal etching were applied to eliminate morphological disorders, to reveal grain boundaries and provide a contrast between grains and grain boundaries.

2.2.3. Dielectric Measurements

Dielectric materials (also called insulators) possess negligible electrical conductivity at room temperature however they are affected by an electric field. If a dielectric material is placed between two plates of the capacitor, the electric field created by capacitors induces a surface charge on the dielectric material, so this increases the charge on the capacitor plates. From the parallel-plate capacitor equation,

$$C\ (Farads) = \frac{\varepsilon\varepsilon_0 A}{d} \tag{2.1}$$

dielectric constant, ε_r, can be derived. Capacitance, C, can be measured experimentally. ε_0 is the electric permittivity of vacuum which is a constant and A and d are surface area and thickness of the material, respectively.(Turton 2000) Capacitance can be experimentally measured by using LCR Meter (Keysight E4980AL). LCR Meter can measure the impedance, Z is the opposition of a circuit offers to the flow of alternating current at a given frequency. Impedance contains real (Resistance, R) and imaginary (Reactance, X) part.

$$Z = R + jX = |Z| \tag{2.2}$$

$$Z = \sqrt{R^2 + X^2} \tag{2.3}$$

$$\theta = \text{atan}\left(\frac{|X|}{R}\right) \tag{2.4}$$

θ represents the phase impedance in terms of angle. If the phase angle θ angle is smaller than zero, reactance becomes capacitive. The LCR meter can read and display the capacitance values of the material. In addition to these parameters, the dissipation factor, D, are used to explain the quality of the materials,

$$\frac{1}{D} = \frac{|X|}{R} \tag{2.5}$$

By using LCR meter and the LabView software, dielectric constant versus temperature data is collected to reveal dielectric properties and structural phase transition characteristics. The calculated dielectric constant value is also called the real part of the dielectric constant. There is another term that defines the dielectric constant: the imaginary part of the dielectric constant. It is known as the loss factor. It shows both energy absorption and how lossy and dissipative a material is. It is proportional to both real part of the dielectric constant and dielectric loss as shown in below the equation of loss tangent (dielectric loss),

$$tan\delta = \frac{\varepsilon^{"}}{\varepsilon'} \tag{2.6}$$

Where $\varepsilon^{"}$ is the imaginary part and ε' is the real part. From this equation, imaginary part versus temperature data were also investigated.(Poole and Darwazeh 2015) Data were collected at different frequencies (0.1,1,10,100 kHz) to investigate the frequency dependence at a temperature range of 25-250 ºC. Both heating and cooling process is applied to the material with a temperature rate of 2 ºC/min to reveal phase transition behaviour (to check for thermal hysteresis). The sample is placed in a sample holder (aixACCT, TFA 423-7) and a temperature controller was used to change the temperature. ε vs T and D vs T data were collected.

2.2.4. Ferroelectric and Electrocaloric Measurements

Ferroelectric properties and electrocaloric effect can be investigated by using polarization hysteresis loops and strain loops. To characterize these hysteresis loops, sample is placed in the sample holder. With the help of a high voltage amplifier (TREK 610E), an electric field is created. Polarization, strain, and current data are collected by Aixplorer software of AixaCCT TF Analyzer 1000 Ferroelectric Tester. Measurements were done at 10 Hz for all samples with silver electrodes. During the electrical measurements, sample holder is filled with silicone oil to prevent the formation of electric arcs. Ferroelectric properties such as coercive electric field, remnant and maximum polarizations, shape of the loop which gives information about ferroelectric and physical

behaviour were investigated. Also, the data of polarization vs. electric field in different temperatures were taken to see how ferroelectric properties are changed due to the temperature. These data were also used to evaluate electrocaloric effect by using Maxwell relations (also called indirect method of electrocaloric measurements). The polarization values of each temperature were collected at same electric field. Numerical equations were used to calculate the electrocaloric effect (or temperature change, ΔT)

2.2.5. Density Measurements

Densities of the samples were measured by using Archimede's principle. The sample is submerged in a fluid and immersed in it. The fluid produces a buoyant upward force and gravitational force acts upon the sample. If we consider the pure water is the fluid, the buoyant force is equal to gravitational force.

$$F_g = m_f * g \tag{2.7}$$

and

$$F_b = p_f * V_g \tag{2.8}$$

From a basic density equation, $m_f = V * p_w$ where p_w is the water density. The mass of the object in air is $M = pV$ where p is the density of the sample. Apparent mass (mass of the sample fully immersed in water), M_{app}, on the other hand, is equal to difference between the actual weight of the sample and the magnitude of the buoyant force.

$$M_{app} = M_{actual} - F_b \tag{2.9}$$

$$M_w * g = M * g - p_w * V * g \tag{2.10}$$

if $F_b = F_g$

$$M_w = M - p_w * \frac{M}{p} \tag{2.11}$$

so $p = \frac{M}{M - M_w} * p_w$

If we consider $p_w = 1\ g/cm^3$, equation becomes,

$$p = \frac{M}{M - M_w} \tag{2.12}$$

All the density measurements were done by using density determination kit of Radurag – AS220 R2 analytical balance. Firstly, masses of the pellets were weighed in air. Then, they are fully immersed in pure water at room temperature. After obtaining values, calculations are done.

CHAPTER 3

RESULTS AND DISCUSSION

3.1. Phase Analysis

Phase analysis of all compositions of BT-NBT system was conducted by X-ray Diffractometer. X-ray diffraction patterns were collected after sintering process of the compositions using ground powder. Pattern was collected between 20^o – 80^o. Analysis was conducted at room temperature. Figure 3.1(a)-(b) illustrates the room temperature XRD patterns of different compositions at the range of 20^o – 80^o and 44^o – 48^o. As shown in Figure 3a, no impurity peaks were observed for any compositions after sintering. This shows that the pure perovskite phase is formed. Figure 3.1b shows (002) (left) and (200) (right) peaks in the XRD pattern directly related to tetragonality in the crystal structure. Double peak at 45^o corresponds to tetragonality and for undoped composition (x=0), tetragonality is maintained. When the amount of Zr doping into B-site was increased, (002) peak gradually disappears thus tetragonality also decreases. Zr having a higher ionic radius (0.72 Å) than titanium (0.605 Å)(Shannon 1976) causes the decrease in tetragonality in crystal structure. In undoped composition, tetragonal peak splitting is very sharp. This implies tetragonal symmetry. In 4% Zr doping, (002) peak is barely seen, and peak splitting is decreased. In 5% Zr doping, intensity of (002) peak is very low. In 45^o, only one peak is observed so tetragonal structure transformed into cubic structure. This change could be associated with larger Zr ionic radius.(Asbani et al. 2015)

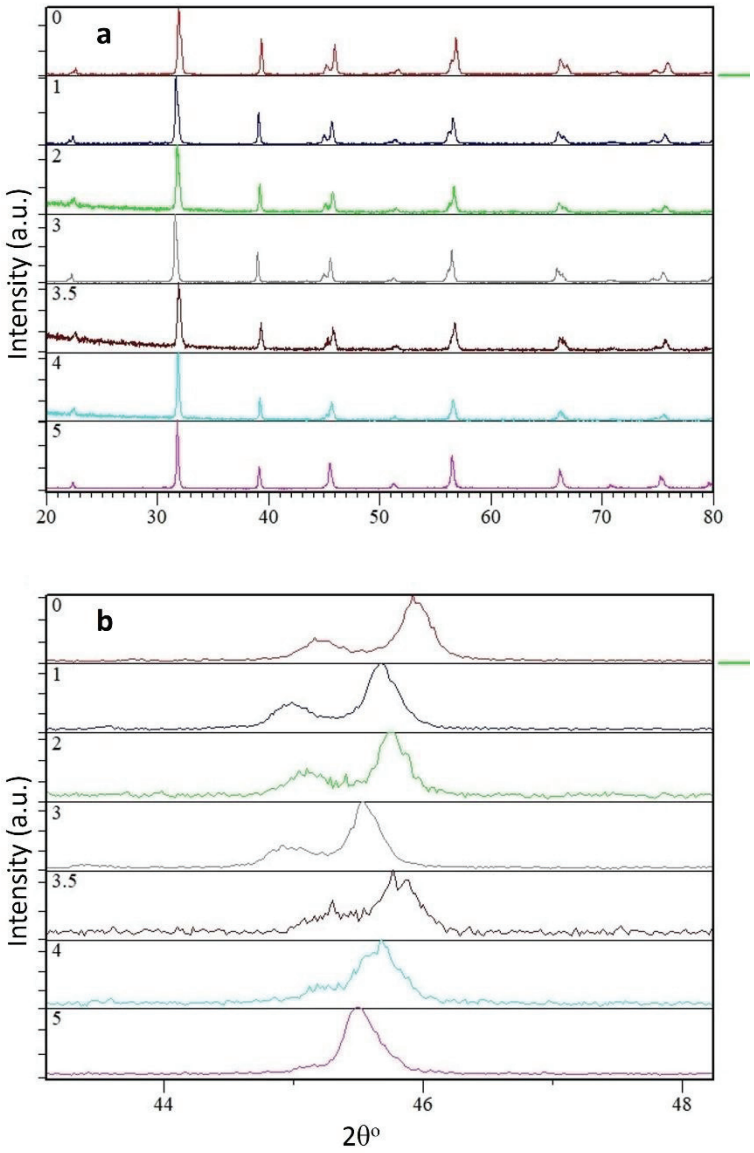

Figure 3.1. XRD patterns of $Ba_{0.7}Na_{0.15}Bi_{0.15}Ti_xZr_{1-x}O_3$ ceramics where x =0.00, 0.01, 0.02, 0.03, 0.035, 0.04 and 0.05 compositions in the range between a) 20° - 80° and b) 44° - 48°.

3.2. Microstructural Analysis

Microstructural analysis of ceramic compositions was done by Scanning Electron Microscopy. BZT-NBT ceramics were thermally etched for revealing the grains. All compositions have relatively dense microstructures. Zr substitution into B-site increases gradually the grain size. Average grain size values are 1,1 μm, 1,2 μm, 1,2 μm, 1,3 μm,

1,3 µm, and 1,5 µm for x=0, 0.01, 0.02, 0.03, 0.035 and 0.05, respectively as shown in Figure 3.2(a)-(f). The changes in the grain size can be attributed to the amounts of Zr doping into B-site within the perovskite structure. Consistent with the literature, increase of the Zr content leads to an increase in grain size.(Asbani et al. 2015)·(Şanlı 2018)

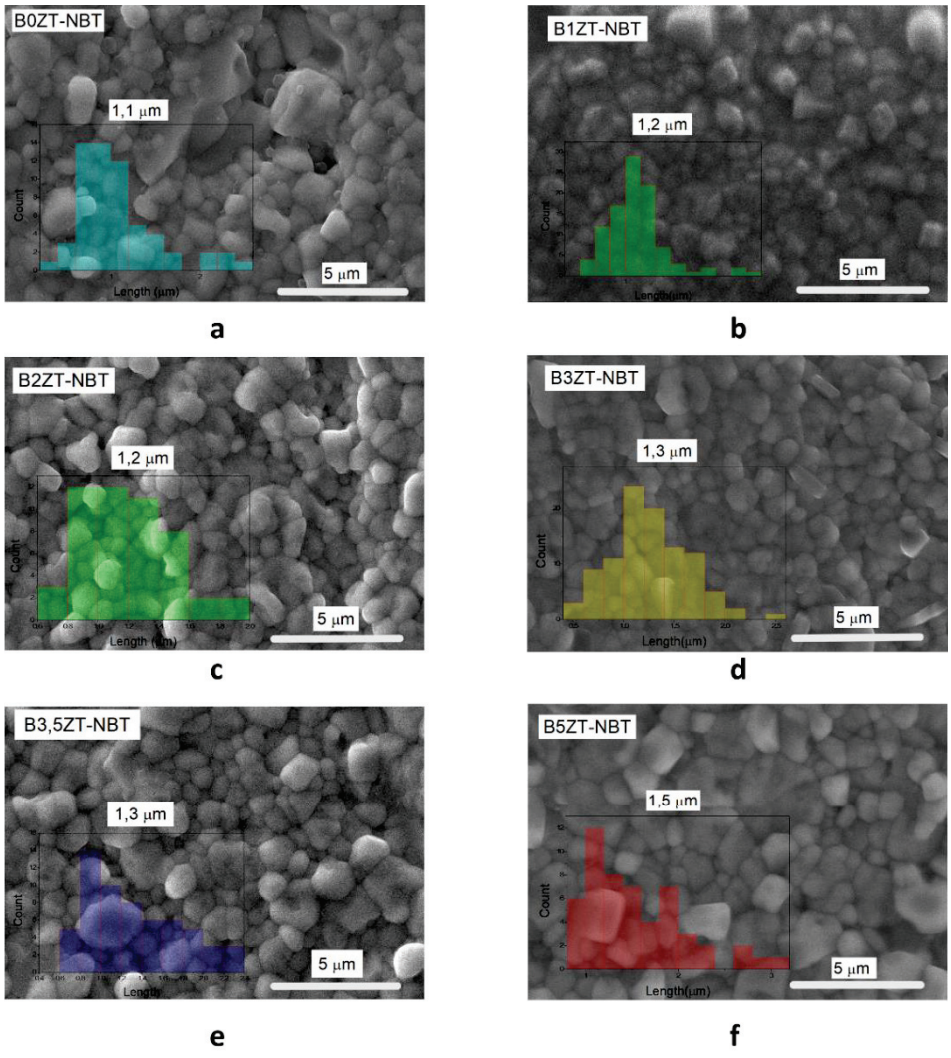

Figure 3.2. SEM images of $Ba_{0.7}Na_{0.15}Bi_{0.15}Ti_xZr_{1-x}O_3$ ceramics where x is a) 0.00, b) 0.01, c) 0.02, d) 0.03, e) 0.035 and f) 0.05 compositions.

3.3. Dielectric Measurements

For each composition, capacitance and dielectric loss values were measured between 25 ºC and 250 ºC by using an LCR meter. Real part (ε) and imaginary part (ε")

of the dielectric constants were calculated by using equations 2.1 and 2.6 as described in section 2.2.3. Temperature dependent dielectric constant and loss values for each ceramic composition at frequencies of 0.1, 1, 10 and 100 kHz are shown in Figure 3.3(a)-(g). From these graphs, assigning a specific Curie point is difficult, even for the undoped sample, as typically a sharp, frequency independent peak is needed. The use of the term maximum dielectric constant (T_m) could be more suitable for these compositions. For the undoped sample as shown in Figure 3.3(a), dielectric peak is sharp and frequency dependence was relatively low. T_m is 183 ºC. Dielectric loss, on the other hand, is relatively high.

Sharp peak behaviour did not change much for x=0, 0.01 and 0.02. However, T_m gradually decreases. For x=0,01 sample, Tm is 177,6 ºC and for x=0,02, Tm is 156,2 ºC. Dielectric constant also was declined with increasing NBT content, but this change is not significant. In x=0.03, frequency dependence can be clearly seen compared to x=0, 0.01 and 0.02. Tm for x=0.03 is around 111.2 ºC. Gradual decrease of Tm point continues. Dielectric constant started to increase in x=0,03. Sharp peak can be seen at frequency of 0,1 kHz. At higher frequencies, peak is broadened and shifted to higher temperatures. This shows the frequency dependence.

For x=0.035, sharp peak turns into broad peak at each frequency. Tm still decreases and its value is 104 ºC. Dielectric loss also decreases while increasing the amount of Zr doping. From undoped composition to x=0.035, dielectric constant graphs show normal ferroelectric behaviour with a relatively weak frequency dependence. This implies that the dielectric behaviour shows the diffuse phase transition rather than first order phase transition, especially in x=0,035.

For x=0.04, and 0.05, as shown in Figure 3.3(f)-(g), behaviour changes very quickly. T_m shift to lower temperatures. T_m is 85,7 ºC and 76,3 ºC for x=0.04 and 0.05, respectively. Frequency dependence was relatively strong for x=0,04 and 0,05. Peaks were broader than other compositions. They are assumed to show relaxor ferroelectric behaviour based on the shift of peak to higher temperatures with increasing frequency. For x=0.05, relaxor behaviour can be seen as strong frequency dependence and broad peak. As Zr doping was increased. T_m is lowered to nearly room temperature. T_m is also strongly dependent on the frequency. In both compositions of x=0.04 and 0.05, T_m is increased when frequency is increased. For example, for x=0.05, T_m temperatures are 76,3 ºC, 83,5 ºC, 98 ºC, 115 ºC for frequencies of 0.1, 1, 10, and 100 kHz, respectively.

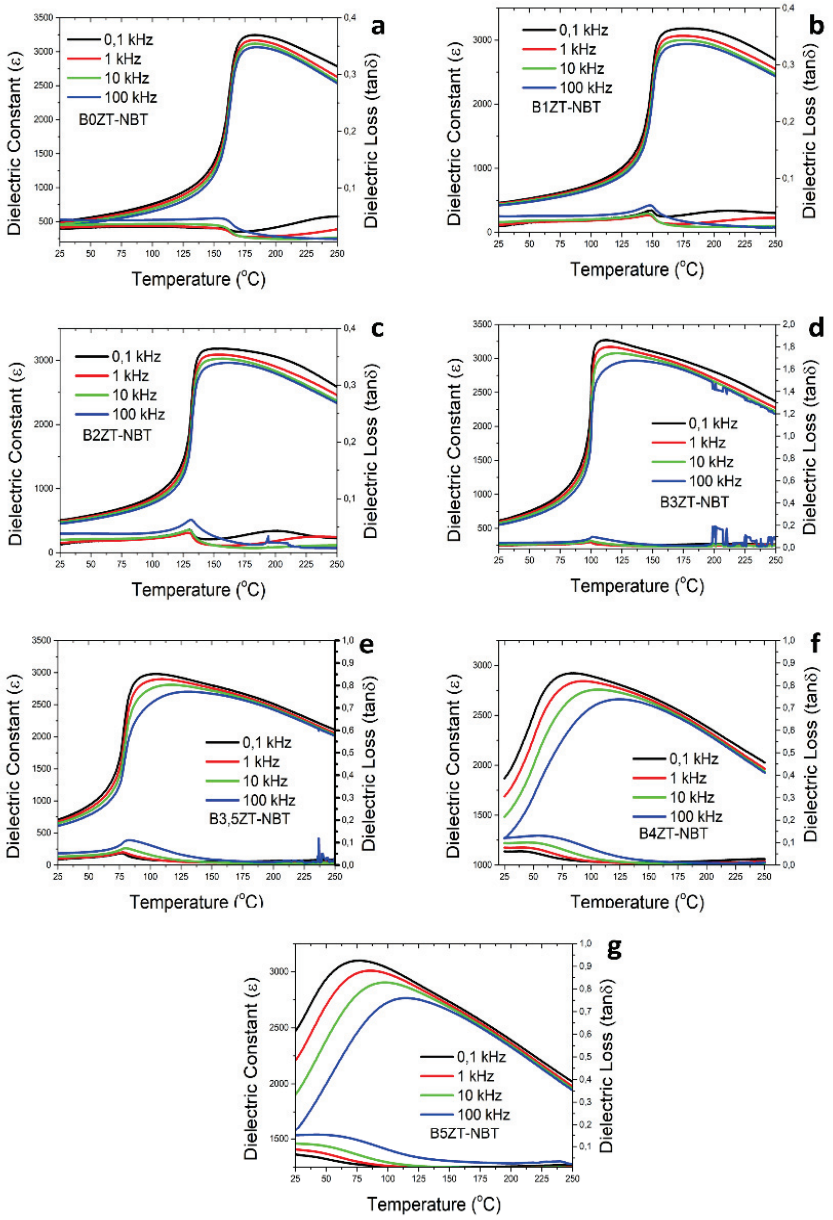

Figure 3.3. Temperature dependence of the dielectric constant and dielectric loss of $Ba_{0.7}Na_{0.15}Bi_{0.15}Ti_xZr_{1-x}O_3$ ceramics where x is a) 0.00, b) 0.01, c) 0.02, d) 0.03, e) 0.035, f) 0.04 and g) 0.05.

Figure 3.4(a)-(c) illustrates the real and imaginary part of dielectric constant and dielectric loss for all compositions. T_m shift to lower temperatures with increasing Zr content can be clearly observed in Figure 3.4(a). In Figure 3.4(b), it can be observed that dielectric loss at room temperature is quite high for x=0.04 and 0.05. A better trend as a function of composition can be seen in Figure 3.4(c). Imaginary part of the dielectric constant increases when the amount of Zr doping was increased. Peaks became broader at high doping amounts and T_m was shifted to lower temperatures.

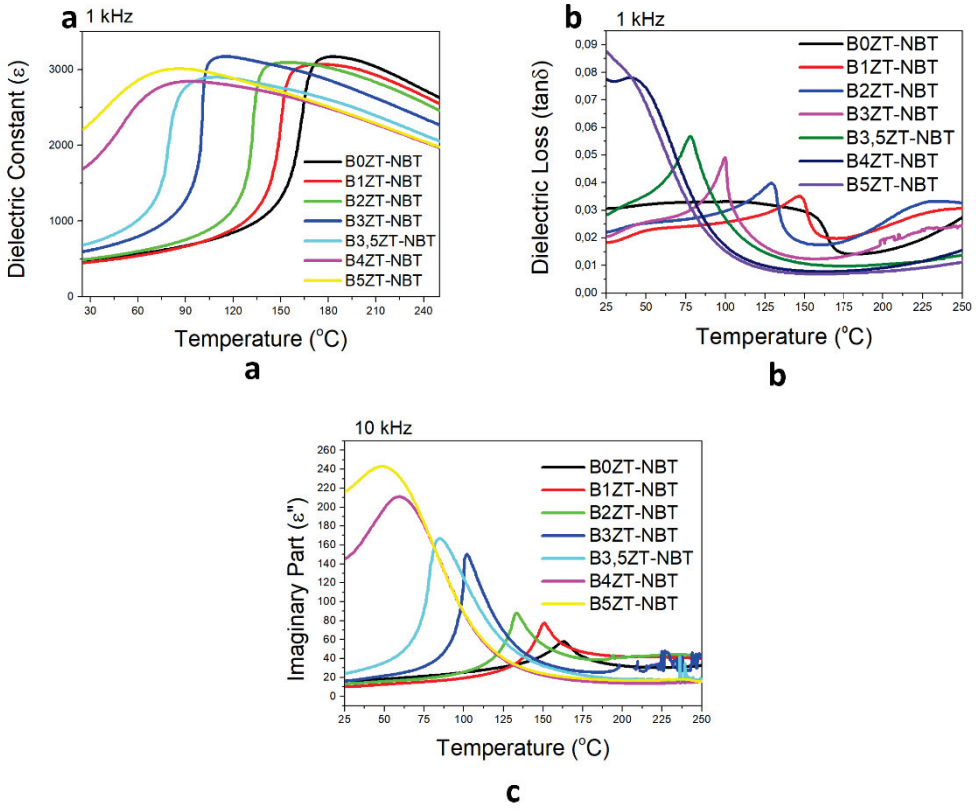

Figure 3.4. Temperature dependence of dielectric constant, dielectric loss, imaginary part of the dielectric constant of of $Ba_{0.7}Na_{0.15}Bi_{0.15}Ti_xZr_{1-x}O_3$ compositions at 1 kHz.

3.4. Ferroelectric Measurements

Ferroelectric measurements were done by using ferroelectric tester with a high voltage amplifier and associated software in a temperature range of 25 °C to 250 °C by using temperature controller. Figure 3.5(a)-(g) illustrates temperature dependent polarization – electric field graphs. Measurements were done at 10 kHz and 40 kV/cm for each temperature. Coercive electric field decreases when temperature is increased. The same case applies to remnant polarization. When temperature was getting much higher, remnant polarization was decreased.

As discussed in Section 3.3, Curie temperature (T_c) couldn't be found easily so maximum temperature at dielectric maxima (T_m) was suitable for these compositions. Figure 3.5(a) shows that near T_m and at high temperatures, linear loops could be seen.

This behaviour is associated with ferroelectric to paraelectric phase transition, material lost its ferroelectricity. However, this transition doesn't happen instantaneously. First, double loops were observed and then loops become linear. Especially in Figure 3.5(f)-(g), double loops could be seen clearly. In Figure 3.5(f), at 25 ^{o}C and 41 ^{o}C, normal ferroelectric loops could be seen but at 54 ^{o}C, double loops took place. Just like other compositions, loops became slimmer and finally linear. This double loop behaviour had to be understood clearly.

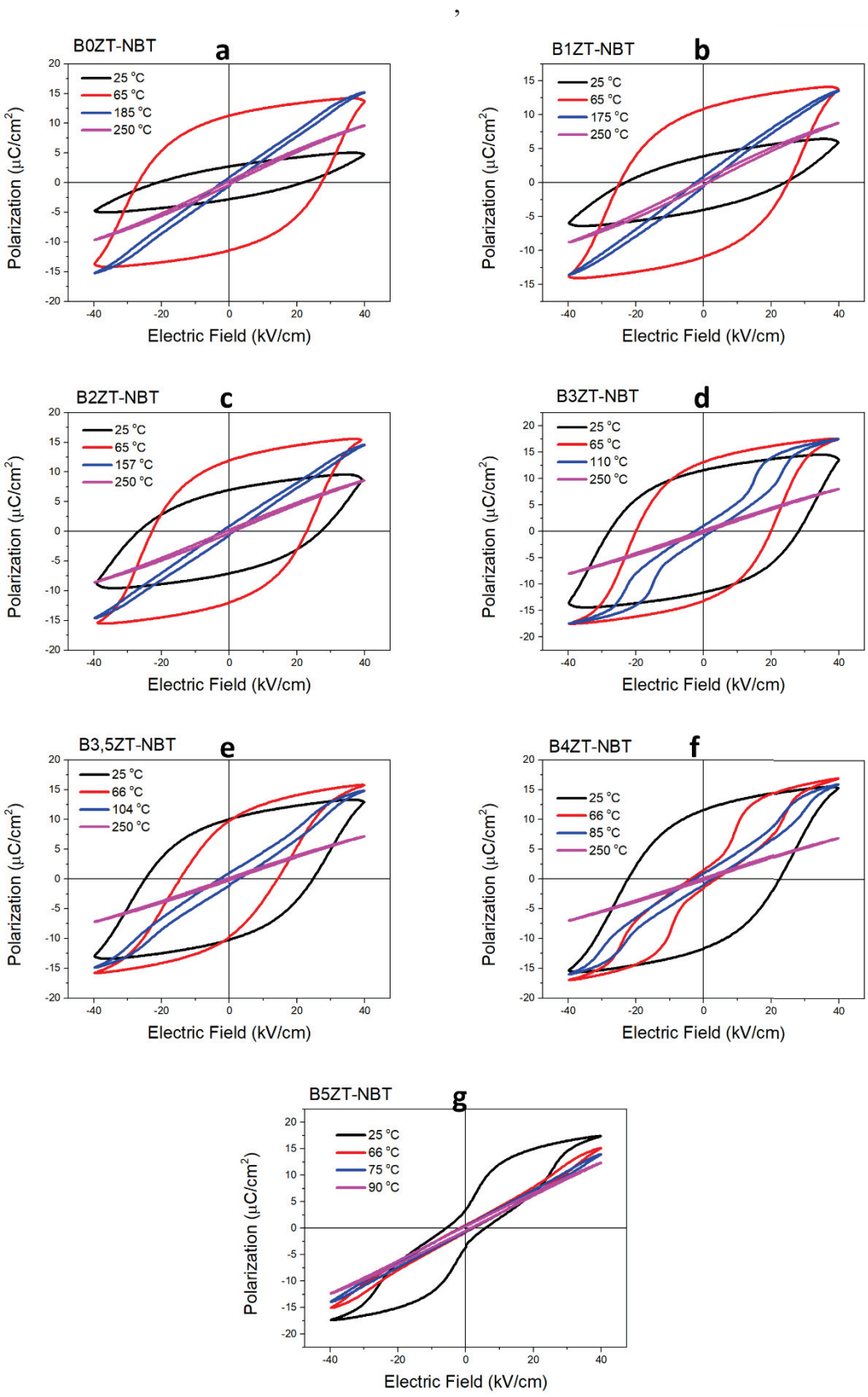

Figure 3.5. Temperature dependent polarization-electric field hysteresis loops of the $Ba_{0.7}Na_{0.15}Bi_{0.15}Ti_xZr_{1-x}O_3$ for x = a) 0.00, b) 0.01, c) 0.02, d) 0.03, e) 0.035, f) 0.04 and g) 0.05 compositions.

Figure 3.6(a)-(g) illustrates temperature dependent strain-electric field relationship. Measurements were done at 10 kHz and 40 kV/cm. As can be seen in all compositions, negative strain decreases as the temperature is increased. Zr doping affected the electric field-induced strain. In Figure 3.6(g) at x= 0.05, except room temperature, there is no negative strain and at the room temperature, negative strain is relatively small. Relaxor behaviour of x=0.05 sample could be the cause of the lack of the negative strain however at room temperature, there is a negative strain, even it was very low. Highest strain of 0.13% is obtained for x=0.04 at 70 ºC as illustrated in Figure 3.6(f).

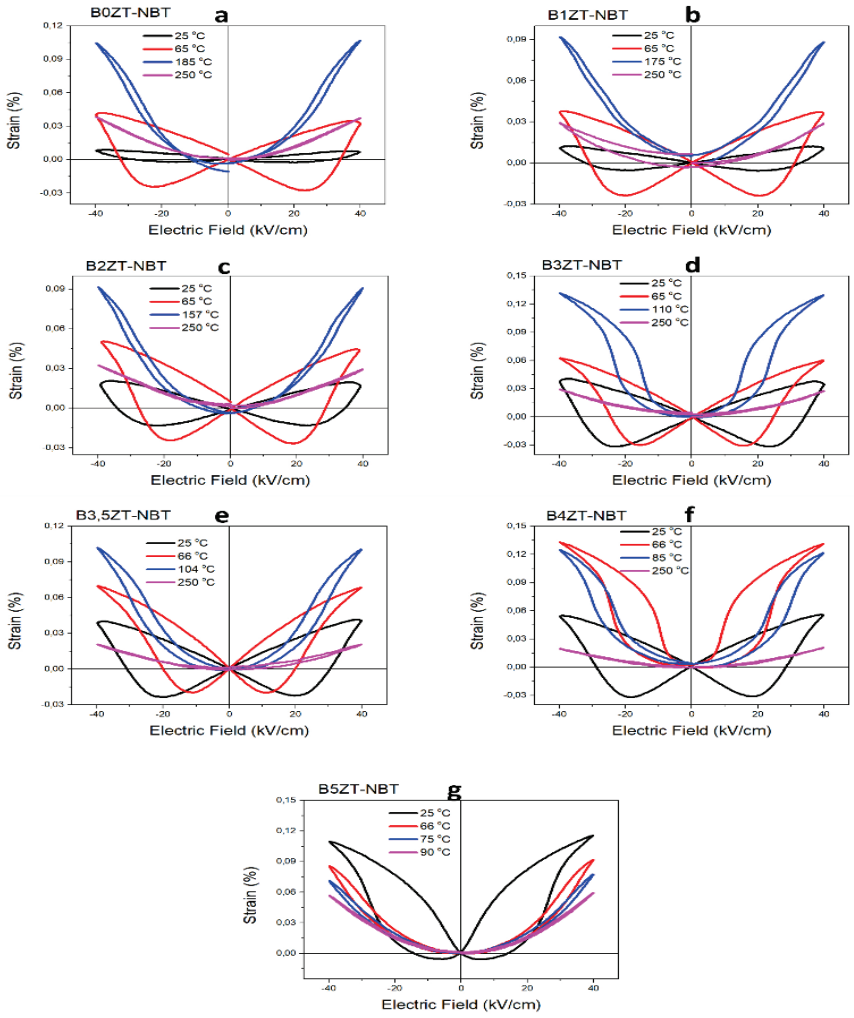

Figure 3.6. Temperature dependent strain-electric field curves of the $Ba_{0.7}Na_{0.15}Bi_{0.15}Ti_xZr_{1-x}O_3$ for x = a) 0.00, b) 0.01, c) 0.02, d) 0.03, e) 0.035, f) 0.04 and g) 0.05 compositions.

To understand the phase transition behaviour of BZT-NBT, further investigation is required. The temperature range where double loops were observed was investigated in detail. In Figure 3.7, double loops of undoped composition could be seen. Double loops were observed at 162 ^{o}C first, below T_m and up to T_m, at higher temperatures double loop becomes linear.

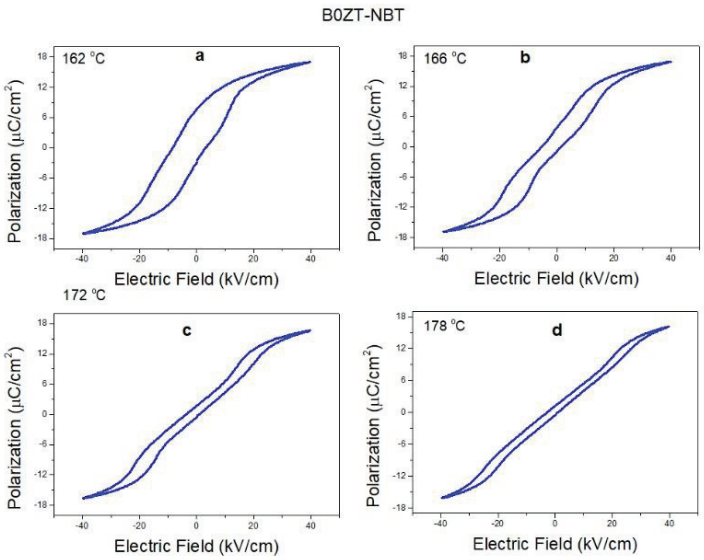

Figure 3.7. Temperature dependent double loops of polarization-electric field graphs of undoped composition.

As shown in Figure 3.8(a)-(d), double loops were started at 148 ^{o}C, 96 ^{o}C, 54 ^{o}C and 25 ^{o}C, where x=0.01, 0.03, 0.04, and 0.5, respectively. Double loops can originate either from the first order phase transition or from ergodic relaxor behaviour. To figure out the exact origin, double loop graphs were insufficient. However, for x=0.05 composition, as seen in Figure 3.8(d), diffuse phase transition is more likely, not because of double loops, but strongly frequency dependent permittivity is a key indicator for relaxors. To understand this behaviour, further explanations were still required.

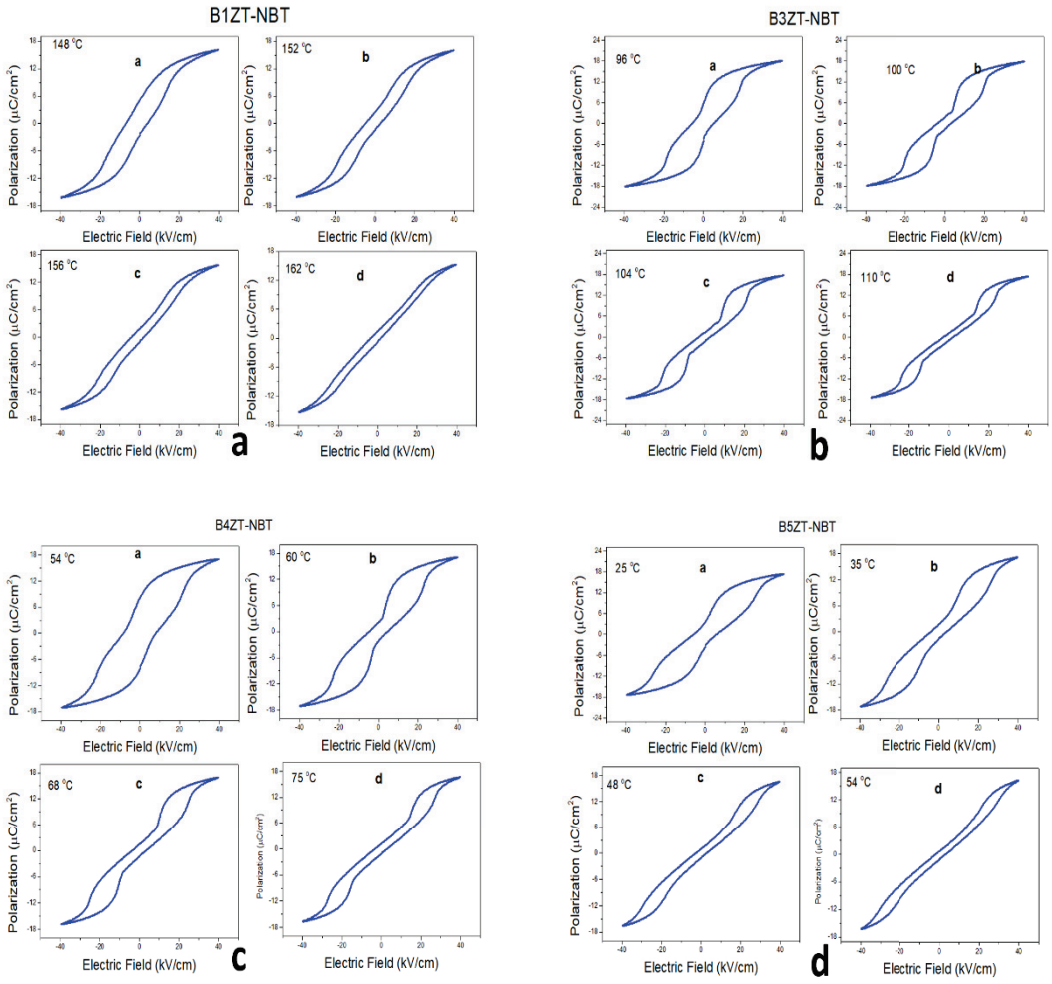

Figure 3.8. Temperature dependent hysteresis loops showing double hysteresis behaviour for $Ba_{0.7}Na_{0.15}Bi_{0.15}Ti_xZr_{1-x}O_3$ where x= a) 0.01, b)0.03, c)0.04, d)0.05

Figure 3.9(a)-(b) shows that hysteresis loops and field-induced strain curves for all compositions measured at 55 kV/cm and 10 kHz at room temperature. Upon zirconium substitution, coercive field decreases. This shows that the domain switching occurs more easily in the presence of Zr doping. This must be related with the decrease in the tetragonality of the material and consequent decrease in T_m. In Figure 3.9(a), there seems to be no distinguished trend between x=0.00 and 0.04 but in 0.05, maximum positive strain of 0.14% and a minimum negative strain of nearly -0.01% could be seen. This is related with the decrease in the T_m towards room temperature. As the transition

temperature is approached, the coercive field decreases, and domain walls can move more easily. This leads to higher contribution from the domain wall motion related strain.

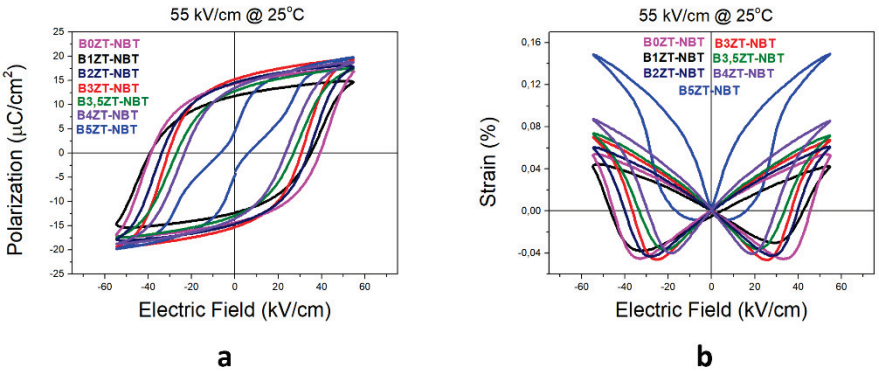

Figure 3.9. Room temperature a) polarization, and b) strain-electric field hysteresis loops comparison for all compositions.

3.5. Electrocaloric Measurements

Electrocaloric temperature change of the samples was estimated by using temperature dependent polarization-electric field data. Indirect method was implemented for the calculations. From these calculations, electric field dependent adiabatic temperature change (ΔT)-temperature graphs were produced. In Figure 3.10(a)-(g), ΔT values are shown. Each composition was measured up to 40 kV/cm up to elevated temperatures. ΔT increased when electric field was increased as expected. Highest ΔT of 2.3 K was obtained for x=0.00 and lowest ΔT of 1.3 K was calculated in x=0.04. T_{span} or temperature range was estimated as the range for which 80% of ΔT_{max} value was maintained. This choice was used in literature too.(Lu et al. 2023a) highest T_{span} values of 10.3 °C and 9.6 °C were found for x=0.035 and 0.04, respectively. Lowest ΔT (x=0.035 and 0.04) has highest T_{span}. Due to the limitation of our setup, the temperature range for dielectric, ferroelectric and electrocaloric measurements was 25 °C to 250 °C. As seen in Figure 3.10. (g), ΔT values of x=0.05 could still rise to higher values at lower temperatures than the room temperature.

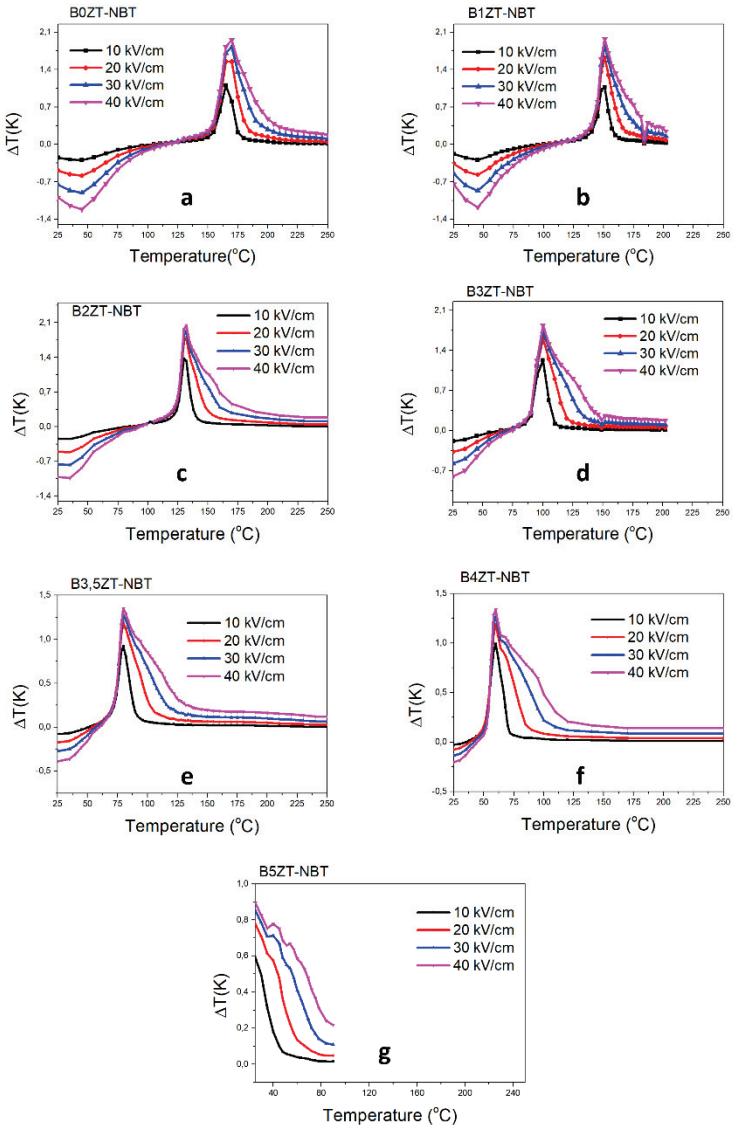

Figure 3.10. Electric field dependent of temperature change (ΔT)-temperature graphs of the $Ba_{0.7}Na_{0.15}Bi_{0.15}Ti_xZr_{1-x}O_3$ for x = a) 0.00, b) 0.01, c) 0.02, d) 0.03, e) 0.035, f) 0.04 and g) 0.05 compositions.

Figure 3.11(a)-(g) illustrates the remnant polarization-temperature relationship for each composition. As discussed in Section 1.3.5, sharp decrease of polarization suggests first-order phase transition. Sudden drop around T_m can be observed in the samples.

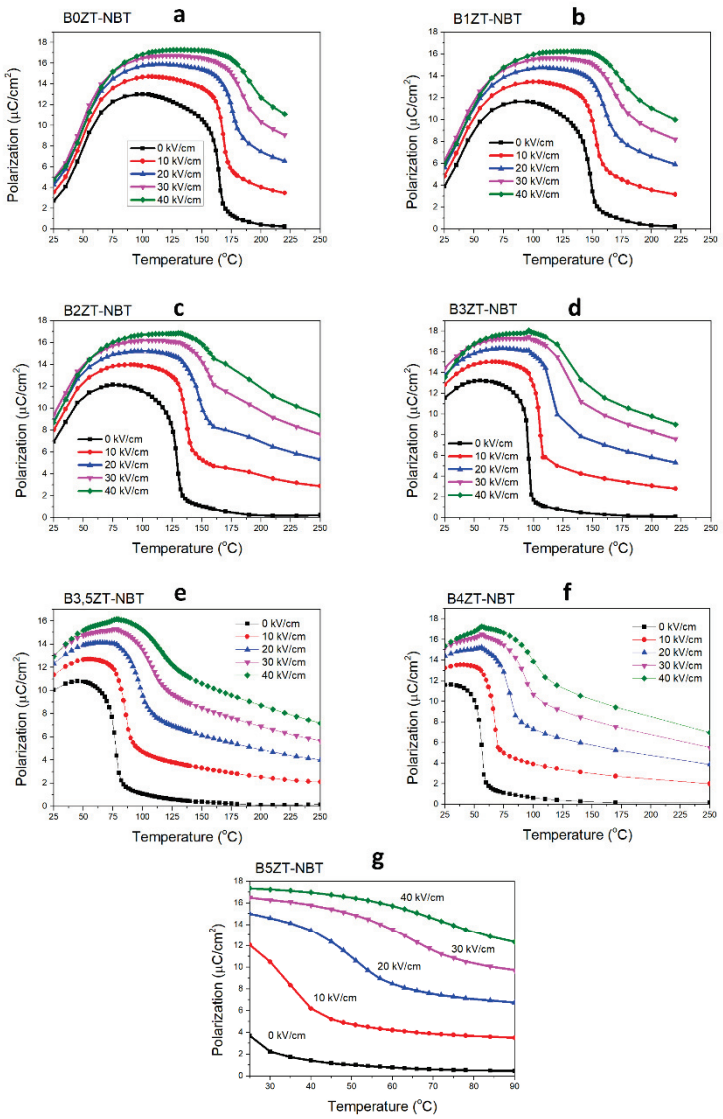

Figure 3.11. Temperature dependent remnant polarization of the $Ba_{0.7}Na_{0.15}Bi_{0.15}Ti_xZr_{1-x}O_3$ for x = a) 0.00, b) 0.01, c) 0.02, d) 0.03, e) 0.035, f) 0.04 and g) 0.05 compositions.

Figure 3.12(a)-(b) shows ΔT vs T and remnant polarization-temperature relationship for all compositions. There is no clear trend in ΔT with Zr substitution, however after x=0.03, ΔT decreases. Also, in Figure 3.12(b), there is no clear trend, but sharp peak in ΔT and sharp decrease in remanent polarization for all samples except x=0.05 suggests first order phase transition character.

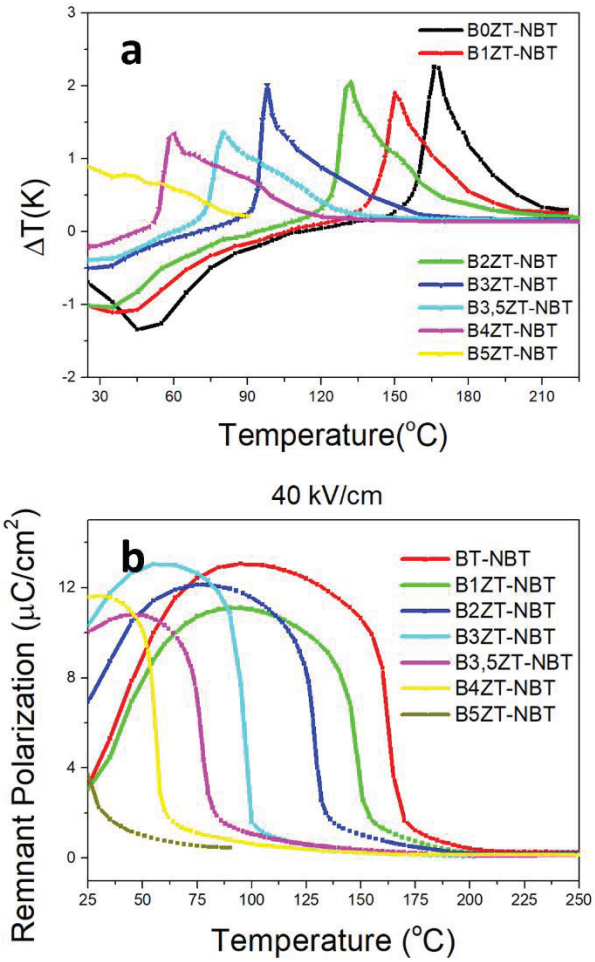

Figure 3.12. Temperature dependent a) ΔT values at 40 kV/cm electric field and b) remnant polarization for all compositions.

Figure 3.13(a)-(g) shows current-electric field relationship. Two peaks are observed for the normal hysteresis loop. Four peaks were observed for double hysteresis loops and when hysteresis loops were slimmer and become linear, peaks cannot be observed in current-electric field curves. As mentioned in the literature(Lu et al. 2023a; 2023b),(Su et al. 2023), ergodic relaxor state can be seen in current-electric field graphs as four peaks are in a four quadrant. In Figure 3.13(a)-(f), at lower temperatures, double peak can be seen and when the temperature is increased to where double loops started, four peaks were present in each quadrant and the distance between peaks are not changed. As expected, when hysteresis loops are getting slimmer, peaks of current are diminished too. In Figure 3.13(g), the behaviour is slightly different. The peaks in first and second quadrant were moving away from each other which was different than other compositions

and four peaks in four quadrants were clearly observed which is a typical feature for ergodic relaxors.(Lu et al. 2023b) Apart from these results, it is still not clear whether the double loops were a result of the relaxor ferroelectric state, however dielectric data for the highest zirconium containing sample (5% mole percent), suggests relaxor ferroelectric behaviour.

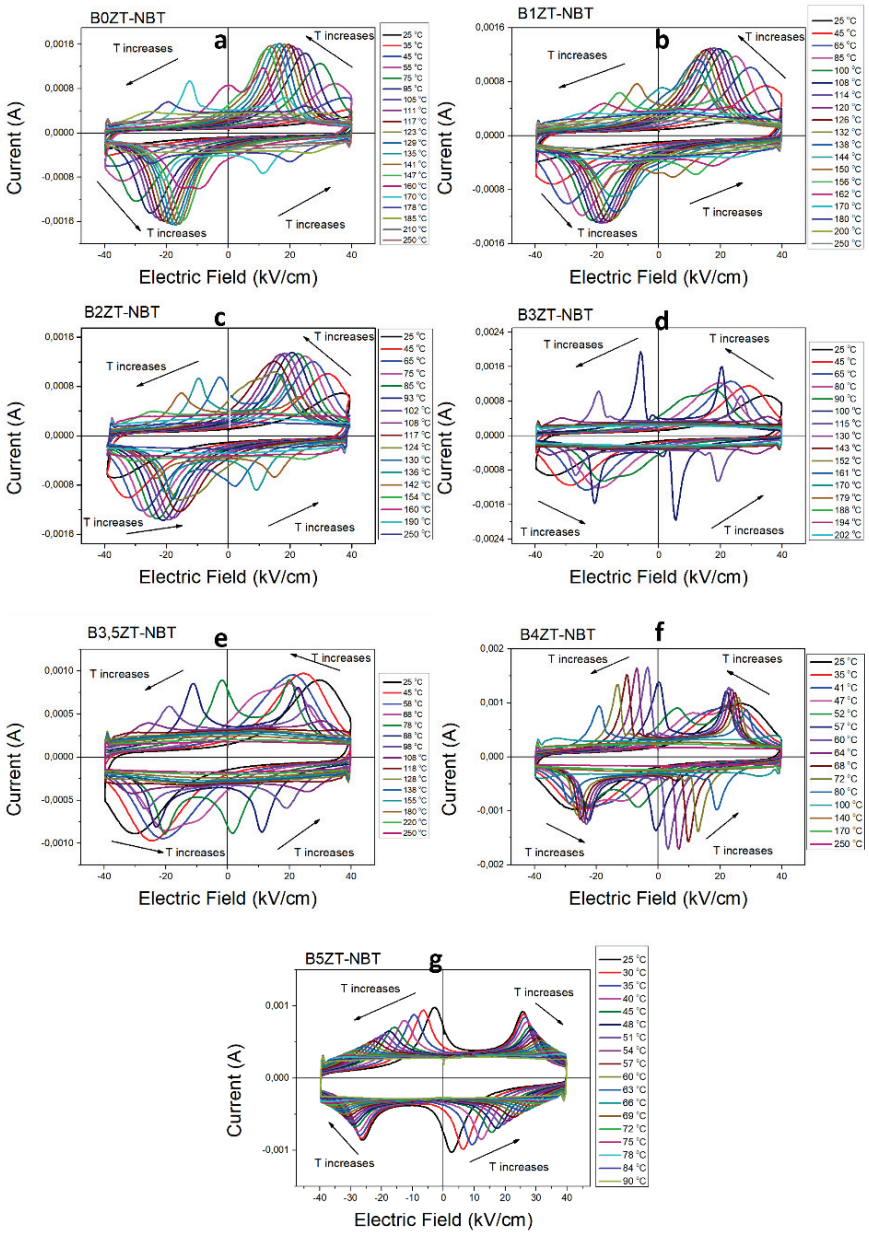

Figure 3.13. Temperature dependent current-electric field of the $Ba_{0.7}Na_{0.15}Bi_{0.15}Ti_xZr_{1-x}O_3$ for x = a) 0.00, b) 0.01, c) 0.02, d) 0.03, e) 0.035, f) 0.04 and g) 0.05 compositions.

Table 3.1 shows that the comparison of electrocaloric properties of compositions of this work and the literature. It can be observed that among the barium titanate-based materials, zirconium doped barium titanate-sodium bismuth titanate systems have promising electrocaloric properties.

Table 3.1. Comparison of electrocaloric properties (ΔT, T_{span} and ΔT/ΔE) of different compositions in both this work and literature.

Composition	$\Delta T(K)$	$T_{span}(°C)$	**ΔT/E (K.m/MV)**	**Method**	**Reference**
B0ZT-NBT	2,3	7,1	0,575	Indirect	This work
B1ZT-NBT	1,9	7,7	0,475	Indirect	This work
B2ZT-NBT	2	7,1	0,500	Indirect	This work
B3ZT-NBT	2	3,8	0,500	Indirect	This work
B3,5ZT-NBT	1,4	10,3	0,350	Indirect	This work
B4ZT-NBT	1,3	9,6	0,325	Indirect	This work
KNLNT-5CZ	0,6	43	0,079	Indirect	(Yang et al. 2020)
PSTZ0,025O3	1,9	8,6	-	Indirect	(Lu et al. 2023a)
BTS-01BCT	0,9	60	-	Direct	(Zhao et al. 2019)
BCZT	1,5	87	0,246	Indirect	(Hanani et al. 2020)
B0,2ZT	4,5	30	0,310	Direct	(Qian et al. 2014)
BT	0,4	10	-	Direct	(Karchevskii 1962b)
P(VDF-TrFE-CFE)	15,7	50	-	Direct	(Li et al. 2011)
BT (single crystal)	1,6	5	-	Direct	(Bai et al. 2012)
$BaTiO_3$	4,8	-	0,480	Indirect	(Bai, Han, Zheng, et al. 2013)

(cont. on next page)

Table 3.1 (cont.)

Composition	$\Delta T(K)$	$T_{span}(°C)$	**ΔT/E (K.m/MV)**	**Method**	**Reference**
$Ba_{0.65}Sr_{0.35}TiO_3$	0.,42		0,210	Indirect	(Bai, Han, Ding, et al. 2013)
$BaZr_{0.05}Ti_{0.95}O_3$	2,4		0,800	Direct	(Jian et al. 2018)
$0.90(BaTiO_3)0.10(Bi_{0.5}Na_{0.5}TiO_3)$	1,30	-	0,325	Indirect	(Karakaya 2022)
$0.80(BaTiO_3)0.20(Bi_{0.5}Na_{0.5}TiO_3)$	2,62	-	0,657	Indirect	(Karakaya 2022)
$0.70(BaTiO_3)0.30(Bi_{0.5}Na_{0.5}TiO_3)$	3,02	-	0,755	Indirect	(Karakaya 2022)
$0.90(BaTiO_3)0.10(Bi_{0.5}Na_{0.5}TiO_3)$	0,90	-	0,225	Direct	-
$080(BaTiO_3)0.20(Bi_{0.5}Na_{0.5}TiO_3)$	2.2	-	0,550	Direct	-

CHAPTER 4

CONCLUSIONS AND SUGGESTIONS FOR THE FUTURE

In this thesis, barium titanate – sodium bismuth titanate solid solutions with different amounts of Zr substitution were synthesized by using solid-state reaction method. $Ba_{0.7}Na_{0.15}Bi_{0.15}Ti_xZr_{1-x}O_3$ composition is studied where x is ranged between 0 % ≤ x ≤ 5 % mol Zr. Phase analysis and microstructural analysis (grain size and morphology) were conducted. Temperature dependent dielectric constant was measured. Ferroelectric and electric field-induced field strain measurements were done as a function of temperature. Indirect electrocaloric measurements by using Maxwell relations were used to investigate adiabatic temperature change ΔT. All samples were phase pure within the accuracy of XRD experiments. Tetragonality of the samples decreased with increasing Zr content, while grain size of the samples increased with Zr-substitution. Furthermore, it was observed that, Zr substitution into Ti-site decreased the Curie temperature and introduced relaxor ferroelectric like behaviour, especially for 4% and 5% mol Zr substitution. However, despite the observation of relaxor characteristics, 1st order nature of the phase transition was maintained for all samples apart from x=0.5, and high ΔT values are obtained at the phase transitions close to room temperature. T_{span} was increased up to 10 °C for 3,5% Zr. Interestingly, Zr substitution does not increase the temperature range in which a large ΔT was observed unlike in $BaTiO_3$. This different behaviour must originate from the peculiar phase transition nature of BT rich BT-NBT solid solution, where increased tetragonality compared to $BaTiO_3$ is likely responsible from the persistent first-order phase transition character. Thermal hysteresis in dielectric and heat flux measurements between heating and cooling is the most conclusive evidence for the first-order phase transition. These experiments should be accurately conducted to reveal the phase transition character in this system.

REFERENCES

Asbani, B, J-L Dellis, A Lahmar, M Courty, M Amjoud, Y Gagou, K Djellab, D Mezzane, Z Kutnjak, and M El Marssi. 2015. “Lead-Free Ba0. 8Ca0. 2 (ZrxTi1− x) O3 Ceramics with Large Electrocaloric Effect.” *Applied Physics Letters* 106 (4).

Bai, Yang, Kai Ding, Guang-Ping Zheng, San-Qiang Shi, and Lijie Qiao. 2012. “Entropy-change Measurement of Electrocaloric Effect of BaTiO3 Single Crystal.” *Physica Status Solidi (a)* 209 (5): 941–44.

Bai, Yang, Xi Han, Kai Ding, and Li-Jie Qiao. 2013. “Combined Effects of Diffuse Phase Transition and Microstructure on the Electrocaloric Effect in {Ba1}−{xSrxTiO3} Ceramics.” *Applied Physics Letters* 103 (16): 162902. https://doi.org/10.1063/1.4825266.

Bai, Yang, Xi Han, Xiu-Cheng Zheng, and Lijie Qiao. 2013. “Both {High} {Reliability} and {Giant} {Electrocaloric} {Strength} in {BaTiO3} {Ceramics}.” *Scientific Reports* 3 (1): 2895. https://doi.org/10.1038/srep02895.

“Barit.” n.d. MTA. https://www.mta.gov.tr/v3.0/bilgi-merkezi/barit) .

Barman, Abhisikta, Sohini Kar-Narayan, and Devajyoti Mukherjee. 2019. “Caloric Effects in Perovskite Oxides.” *Advanced Materials Interfaces* 6 (15): 1900291.

“Bismuth Market - Growth, Trends, COVID-19 Impact, and Forecasts (2023 - 2028).” n.d. Mordor Intelligence. https://www.mordorintelligence.com/industry-reports/bismuth-market.

Callister, W D, and D G Rethwisch. 2014. “Materials and Engineering 9th Edition.” *New York: Jonh Wiley and Sons Inc*.

Cazorla, Claudio. 2019. “Novel Mechanocaloric Materials for Solid-State Cooling Applications.” *Applied Physics Reviews* 6 (4).

Chemicool.com. 2012. “Zirconium.” Chemicool.Com. 2012. https://www.chemicool.com/elements/zirconium.html.

Chu, F, I M Reaney, and N Setter. 1995. “Spontaneous (Zero-Field) Relaxor–to–Ferroelectric-Phase Transition in Disordered {Pb}({Sc1}/{2Nb1}/2){O3}.” *Journal of Applied Physics* 77 (4): 1671–76. https://doi.org/10.1063/1.358856.

Correia, Tatiana, and Qi Zhang. 2014. “Electrocaloric Materials.” *New Generation of Coolers* 34.

Cui, Jun, Yiming Wu, Jan Muehlbauer, Yunho Hwang, Reinhard Radermacher, Sean Fackler, Manfred Wuttig, and Ichiro Takeuchi. 2012. “Demonstration of High Efficiency Elastocaloric Cooling with Large ΔT Using NiTi Wires.” *Applied Physics Letters* 101 (7).

Czaja, P, M Piasecki, M B Zapart, J Suchanicz, K Konieczny, J Michniowski, D Sitko, G Stachowski, and K Kluczewska-Chmielarz. 2020. “Significant Increment of the Dielectric Permittivity and Domain Properties in the (1-x) PbTiO3-x (Na0. 5Bi0. 5) TiO3 Crystals.” *Archives of Metallurgy and Materials*, 163–68.

Dall’Olio, Stefano, M Masche, Jierong Liang, A R Insinga, Dan Eriksen, Rasmus Bjørk, Kaspar K Nielsen, Alexander Barcza, H A Vieyra, and Niels V Beek. 2021. “Novel Design of a High Efficiency Multi-Bed Active Magnetic Regenerator Heat Pump.” *International Journal of Refrigeration* 132: 243–54.

Dekker, Adrianus J. 1981. *Solid {State} {Physics}*. London: Macmillan Education UK. https://doi.org/10.1007/978-1-349-00784-4.

Directive, E U. 2013. “Restriction of the Use of Certain Hazardous Substances in Electrical and Electronic Equipment (RoHS).” *Off. J. Eur. Communities* 46: 19–23.

“Global Sodium Carbonate Market.” 2022. Spherical Insights. 2022. https://www.sphericalinsights.com/reports/sodium-carbonate-market.

Goldstein, JI, DE Newbury, JR Michael, and NWM Ritchie. 2017. “Scanning Electron Microscopy and X-Ray Microanalysis.”

Gomah-Pettry, Jean-Richard, Senda Saïd, Pascal Marchet, and Jean-Pierre Mercurio. 2004. “Sodium-Bismuth Titanate Based Lead-Free Ferroelectric Materials.” *Journal of the European Ceramic Society* 24 (6): 1165–69.

Graef, Marc De, and Michael E McHenry. 2007. *Structure of Materials: An Introduction to Crystallography, Diffraction and Symmetry*. Cambridge: Cambridge University Press.

Hanani, Zouhair, Soukaina Merselmiz, Daoud Mezzane, Andraž Bradeško, Brigita Rožič, Mohammed Lahcini, Mimoun El Marssi, Andrey V Ragulya, Igor A Luk'Yanchuk, and Zdravko Kutnjak. 2020. "Thermally-Stable High Energy Storage Performances and Large Electrocaloric Effect over a Broad Temperature Span in Lead-Free BCZT Ceramic." *RSC Advances* 10 (51): 30746–55.

Hannun, R M, and S Q Hamza. 2021. "Modeling Efficient Hybrid Air Conditioning System." In *Journal of Physics: Conference Series*, 1773:12025. IOP Publishing.

Heath, Eric A. 2017. "Amendment to the Montreal Protocol on Substances That Deplete the Ozone Layer (Kigali Amendment)." *International Legal Materials* 56 (1): 193–205. https://doi.org/10.1017/ilm.2016.2.

Hennings, Detlev, A Schnell, and G Simon. 1982. "Diffuse Ferroelectric Phase Transitions in Ba (Ti1-yZry) O3 Ceramics." *Journal of the American Ceramic Society* 65 (11): 539–44.

Jian, Xiao-Dong, Biao Lu, Dan-Dan Li, Ying-Bang Yao, Tao Tao, Bo Liang, Jin-Hong Guo, Yi-Jiang Zeng, Jia-Le Chen, and Sheng-Guo Lu. 2018. "Direct Measurement of Large Electrocaloric Effect in Ba (Zr x Ti1–x) O3 Ceramics." *ACS Applied Materials & Interfaces* 10 (5): 4801–7.

Karakaya, Merve. 2022. "Lead-Free Ferroelectric Ceramics for Energy Storage and Electrocaloric Cooling Applications."

Karchevskii, A I. 1962a. "Electrocaloric Effect in Polycrystalline Barium Titanate." *Soviet Physics-Solid State* 3 (10): 2249–54.

———. 1962b. "Electrocaloric Effect in Polycrystalline Barium Titanate." *Soviet Physics-Solid State* 3 (10): 2249–54.

Katz, Eugene A. 2020. "Perovskite: Name Puzzle and German-Russian Odyssey of Discovery." *Helvetica Chimica Acta* 103 (6): e2000061.

Kiran Pulidindi, Kunal Ahuja. 2023. "Zirconium Market."

Kirillov, V V, and V A Isupov. 1973. “Relaxation Polarization of PbMg 1/3Nb2/3O3 (PMN)-A Ferroelectric with a Diffused Phase Transition.” *Ferroelectrics* 5 (1): 3–9.

Li, Xinyu, Xiao-shi Qian, S G Lu, Jiping Cheng, Zhao Fang, and Q M Zhang. 2011. “Tunable Temperature Dependence of Electrocaloric Effect in Ferroelectric Relaxor Poly (Vinylidene Fluoride-Trifluoroethylene-Chlorofluoroethylene Terpolymer.” *Applied Physics Letters* 99 (5).

Lines, Malcolm E, and Alastair M Glass. 2001. *Principles and Applications of Ferroelectrics and Related Materials*. Oxford university press.

Liu, Yang, James F Scott, and Brahim Dkhil. 2016. “Direct and Indirect Measurements on Electrocaloric Effect: Recent Developments and Perspectives.” *Applied Physics Reviews* 3 (3).

Lu, Yanzhou, Xiaofan Sun, Min Zhao, Shulin Jiao, Dong Li, Peng Chen, Wentao Zhang, Kongmeng Ye, Libo Xu, and Qi You. 2023a. “Enhanced Electrocaloric Effect of Lead Scandium Tantalate by Zirconium Doping.” *ACS Applied Materials & Interfaces*.

———. 2023b. “Enhanced Electrocaloric Effect of Lead Scandium Tantalate by Zirconium Doping.” *ACS Applied Materials & Interfaces*.

Ma, Rujun, Ziyang Zhang, Kwing Tong, David Huber, Roy Kornbluh, Yongho Sungtaek Ju, and Qibing Pei. 2017. “Highly Efficient Electrocaloric Cooling with Electrostatic Actuation.” *Science* 357 (6356): 1130–34.

Merz, Walter J. 1953. “Double {Hysteresis} {Loop} of {BaTi} {O} 3 at the {Curie} {Point}.” *Physical Review* 91 (3): 513–17. https://doi.org/10.1103/PhysRev.91.513.

Mischenko, A S, Qi Zhang, J F Scott, R W Whatmore, and N D Mathur. 2006. “Giant Electrocaloric Effect in Thin-Film PbZr0. 95Ti0. 05O3.” *Science* 311 (5765): 1270–71.

Mischenko, A S, Qi Zhang, Roger W Whatmore, J F Scott, and N D Mathur. 2006. “Giant Electrocaloric Effect in the Thin Film Relaxor Ferroelectric 0.9 PbMg1⁄3Nb2⁄3O3–0.1 PbTiO3 near Room Temperature.” *Applied Physics Letters* 89 (24).

Mo, Frode, Ragnvald H Mathiesen, Jon Are Beukes, and Khanh Minh Vu. 2015. "Rochelle Salt–a Structural Reinvestigation with Improved Tools. I. The High-Temperature Paraelectric Phase at 308 K." *IUCrJ* 2 (1): 19–28.

Mordor Intelligence Research & Advisory. 2023. "Zirconium Market Size & Share Analysis - Growth Trends & Forecasts (2023 - 2028)." Mordor Intelligence. 2023. https://www.mordorintelligence.com/industry-reports/zirconium-market Source: https://www.mordorintelligence.com/industry-reports/zirconium-market.

Nakashima, Yoshifumi, Wataru Sakamoto, Tetsuo Shimura, and Toshinobu Yogo. 2007. "Chemical {Processing} and {Characterization} of {Ferroelectric} ({K},{Na}){NbO3} {Thin} {Films}." *Japanese Journal of Applied Physics* 46 (10S): 6971. https://doi.org/10.1143/JJAP.46.6971.

Neese, Bret, Baojin Chu, Sheng-Guo Lu, Yong Wang, E Furman, and Q M Zhang. 2008. "Large Electrocaloric Effect in Ferroelectric Polymers near Room Temperature." *Science* 321 (5890): 821–23.

"Net Zero Roadmap: A Global Pathway to Keep the 1.5 °C Goal in Reach." 2023.

Nguyen, Minh D, Chi T Q Nguyen, Hung N Vu, and Guus Rijnders. 2019. "Experimental Evidence of Breakdown Strength and Its Effect on Energy-Storage Performance in Normal and Relaxor Ferroelectric Films." *Current Applied Physics* 19 (9): 1040–45.

Nouchokgwe, Youri, Pierre Lheritier, Chang-Hyo Hong, Alvar Torelló, Romain Faye, Wook Jo, Christian R H Bahl, and Emmanuel Defay. 2021. "Giant Electrocaloric Materials Energy Efficiency in Highly Ordered Lead Scandium Tantalate." *Nature Communications* 12 (1): 3298.

Pandey, R Kumar. 2019. *Fundamentals of Electroceramics: Materials, Devices, and Applications*. John Wiley \& Sons.

Park, Jiwon, Dong-Gyu Lee, Sunghoon Hur, Jeong Min Baik, Hyun Soo Kim, and Hyun-Cheol Song. 2023. "A Review on Recent Advances in Piezoelectric Ceramic 3D Printing." In *Actuators*, 12:177. MDPI.

Peng, Biaolin, Huiqing Fan, and Qi Zhang. 2013. "A Giant Electrocaloric Effect in Nanoscale Antiferroelectric and Ferroelectric Phases Coexisting in a Relaxor Pb0.

8Ba0. 2ZrO3 Thin Film at Room Temperature." *Advanced Functional Materials* 23 (23): 2987–92.

"Piezoelectric Balance Presented by Pierre Curie to Lord Kelvin, Hunterian Museum, Glasgow." n.d. Wikimedia.

Poole, Clive, and Izzat Darwazeh. 2015. *Microwave Active Circuit Analysis and Design*. Academic Press.

Qian, Xiao-Shi, Hui-Jian Ye, Ying-Tang Zhang, Haiming Gu, Xinyu Li, C A Randall, and Q M Zhang. 2014. "Giant {Electrocaloric} {Response} {Over} {A} {Broad} {Temperature} {Range} in {Modified} {BaTiO3} {Ceramics}." *Advanced Functional Materials* 24 (9): 1300–1305. https://doi.org/10.1002/adfm.201302386.

Qin, Yongxin, Bingchao Qin, Dongyang Wang, Cheng Chang, and Li-Dong Zhao. 2022. "Solid-State Cooling: Thermoelectrics." *Energy & Environmental Science*.

Radebaugh, R, W N Lawless, J D Siegwarth, and A J Morrow. 1979. "Feasibility of Electrocaloric Refrigeration for the 4–15 K Temperature Range." *Cryogenics* 19 (4): 187–208.

Rödel, Jürgen, Wook Jo, Klaus T P Seifert, Eva-Maria Anton, Torsten Granzow, and Dragan Damjanovic. 2009. "Perspective on the {Development} of {Lead}-Free {Piezoceramics}." *Journal of the American Ceramic Society* 92 (6): 1153–77. https://doi.org/10.1111/j.1551-2916.2009.03061.x.

Sakayori, Ken-ichi, Yasunori Matsui, Hiroyuki Abe, Eiji Nakamura, Mikihiko Kenmoku, Tomoyuki Hara, Daisuke Ishikawa, Akihiro Kokubu, Ken-ichi Hirota, and Takuro Ikeda Takuro Ikeda. 1995. "Curie Temperature of BaTiO3." *Japanese Journal of Applied Physics* 34 (9S): 5443.

Şanlı, Keriman. 2018. "BaTiO 3 Based Ferroelectric Materials for Electrocaloric Cooling Applications." Izmir Institute of Technology (Turkey).

Sattar, M A, Rahman Saidur, and Haji Hassan Masjuki. 2007. "Performance Investigation of Domestic Refrigerator Using Pure Hydrocarbons and Blends of Hydrocarbons as Refrigerants."

Scott, J F. 2007. “Applications of {Modern} {Ferroelectrics}.” *Science* 315 (5814): 954–59. https://doi.org/10.1126/science.1129564.

Shah, Nihar, Max Wei, Virginie Letschert, and Amol Phadke. 2015. “Benefits of {Leapfrogging} to {Superefficiency} and {Low} {Global} {Warming} {Potential} {Refrigerants} in {Room} {Air} {Conditioning}.” https://doi.org/10.2172/1397235.

Shannon, Robert D. 1976. “Revised Effective Ionic Radii and Systematic Studies of Interatomic Distances in Halides and Chalcogenides.” *Acta Crystallographica Section A: Crystal Physics, Diffraction, Theoretical and General Crystallography* 32 (5): 751–67.

Shebanov, L, and K Borman. 1992. “On Lead-Scandium Tantalate Solid Solutions with High Electrocaloric Effect.” *Ferroelectrics* 127 (1): 143–48.

Shi, Junye, Donglin Han, Zichao Li, Lu Yang, Sheng-Guo Lu, Zhifeng Zhong, Jiangping Chen, Q M Zhang, and Xiaoshi Qian. 2019. “Electrocaloric Cooling Materials and Devices for Zero-Global-Warming-Potential, High-Efficiency Refrigeration.” *Joule* 3 (5): 1200–1225.

Shvartsman, Vladimir V, and Doru C Lupascu. 2012. “Lead-{Free} {Relaxor} {Ferroelectrics}.” Edited by D J Green. *Journal of the American Ceramic Society* 95 (1): 1–26. https://doi.org/10.1111/j.1551-2916.2011.04952.x.

Staley, Dean Mitchell, C W Bullard, and R R Crawford. 1992. “Steady-State Performance of a Domestic Refrigerator/Freezer Using R12 and R134a.” *Air Conditioning and Refrigeration Center TR-22*.

Su, Xiaopo, Junjie Li, Yuxuan Hou, Ruowei Yin, Jianting Li, Shiqiang Qin, Yanjing Su, Lijie Qiao, Chuanbao Liu, and Yang Bai. 2023. “Large Electrocaloric Effect over a Wide Temperature Span in Lead-Free Bismuth Sodium Titanate-Based Relaxor Ferroelectrics.” *Journal of Materiomics* 9 (2): 289–98.

Suchanicz, J, D Sitko, N-TH Kim-Ngan, and A G Balogh. 2008. “Electric Properties of Soft PZT Ceramics under Combined Electric and Mechanic Fields.” *Journal of Applied Physics* 104 (9).

"Titanium Market Size & Share Analysis - Growth Trends & Forecasts (2023 - 2028)." n.d. Mordor Intelligence. https://www.mordorintelligence.com/industry-reports/titanium-alloy-market.

Torelló, Alvar, and Emmanuel Defay. 2022. "Electrocaloric {Coolers}: {A} {Review}." *Advanced Electronic Materials* 8 (6): 2101031. https://doi.org/10.1002/aelm.202101031.

Turton, Richard. 2000. *The Physics of Solids*. Oxford ; New York: Oxford University Press.

Tuttle, B A, and D A Payne. 1981. "The Effects of Microstructure on the Electrocaloric Properties of Pb (Zr, Sn, Ti) O3 Ceramics." *Ferroelectrics* 37 (1): 603–6.

"Understanding How Efficient Your Air Conditioner Is." n.d. Atlantis Solar. https://www.atlantissolar.com/cop_eer.html.

Walsh, Aron, and Graeme W Watson. 2005. "The Origin of the Stereochemically Active Pb (II) Lone Pair: DFT Calculations on PbO and PbS." *Journal of Solid State Chemistry* 178 (5): 1422–28.

Whatmore, Roger. 2017. "Ferroelectric {Materials}." In *Springer {Handbook} of {Electronic} and {Photonic} {Materials}*, edited by Safa Kasap and Peter Capper, 1. Springer {Handbooks}. Cham: Springer International Publishing. https://doi.org/10.1007/978-3-319-48933-9_26.

Yang, Junlin, Ye Zhao, Xiaojie Lou, Jiagang Wu, and Xihong Hao. 2020. "Synergistically Optimizing Electrocaloric Effects and Temperature Span in KNN-Based Ceramics Utilizing a Relaxor Multiphase Boundary." *Journal of Materials Chemistry C* 8 (12): 4030–39.

Yin, Jie, Yuxing Zhang, Xiang Lv, and Jiagang Wu. 2018. "Ultrahigh Energy-Storage Potential under Low Electric Field in Bismuth Sodium Titanate-Based Perovskite Ferroelectrics." *Journal of Materials Chemistry A* 6 (21): 9823–32. https://doi.org/10.1039/C8TA00474A.

Yoon, Seok-Hyun, Mi-Yang Kim, and Donghun Kim. 2017. "Influence of Tetragonality (c/a) on Dielectric Nonlinearity and Direct Current (Dc) Bias Characteristics of (1-x) BaTiO3-XBi0. 5Na0. 5TiO3 Ceramics." *Journal of Applied Physics* 122 (15).

Zhao, Chunlin, Junlin Yang, Yanli Huang, Xihong Hao, and Jiagang Wu. 2019. “Broad-Temperature-Span and Large Electrocaloric Effect in Lead-Free Ceramics Utilizing Successive and Metastable Phase Transitions.” *Journal of Materials Chemistry A* 7 (44): 25526–36.

Zheng, Mupeng, Changhao Zhao, and Jürgen Rödel. 2023. “Transitions from Soft to Hard Piezoelectricity of ({Ba}, {Ca})({Ti}, {Zr}){O3} Ceramics via Precipitation Hardening.” *Applied Physics Letters* 122 (13): 132904. https://doi.org/10.1063/5.0146096.

Zheng, Xiu-Cheng, Guang-Ping Zheng, Zheng Lin, and Zhi-Yuan Jiang. 2012. “Electro-Caloric Behaviors of Lead-Free Bi 0.5 Na 0.5 TiO 3-BaTiO 3 Ceramics.” *Journal of Electroceramics* 28: 20–26.